Evaluating Forest Degradation in the Kurdistan Region of Iraq Utilizing Remote Sensing and Geographic Information Systems (GIS)

Nechirvan Shafeh Othman[1*], Heman Abdulkhaleq A. Gaznayee[2]

[1]Department of Forest, College of Agricultural Engineering Sciences, Salahaddin University-Erbil, Kurdistan Region, Iraq.

heman.ahmed@su.edu.krd , nechervanshafih@gmail.com

*Corresponding author email: nechervanshafih@gmail.com

Abstract

Forests in the Kurdistan Region of Iraq are crucial for ecological balance, biodiversity, and local livelihoods. These forests face growing threats from natural and human causes, including climate change, agricultural expansion, overgrazing, and illegal logging. This research examines how forest area and plant health changed from 2016 to 2024 across approximately 46,781 km² in KRI, using NDVI to map land cover and dNBR to assess fire damage. We used multiple linear regression and PCA to examine relationships between NDVI and factors such as elevation, rainfall, temperature, slope, humidity, and fire severity, both regionally and within four governorates (Erbil, Sulaymaniyah, Duhok, and Halabja). Overall, forest land increased from 19.2% (8,970.9 km²) in 2016 to 22.4% (10,471.2 km²) in 2024, peaking at 25.2% (11,797.2 km²) in 2019 and bottoming at 18.0% (8,401.0 km²) in 2022, indicating significant year-to-year variation. Analysis of Precipitation and forest cover found that the wettest period (2018–2019; 1,169.8 mm) matched the maximum regional forest extent and the smallest forest loss (0.8%). Conversely, the driest period (2020–2021; 372.2 mm) saw the highest forest loss (5.0%) and the steepest decline, indicating that much of the observed forest change is climate-related variation in greenness rather than permanent land conversion. Correlation analysis showed strong positive links between DEM and precipitation (r=0.641), DEM and slope (r=0.632), and NDVI and rainfall (r=0.540). Negative relationships were found between temperature and both precipitation (r = -0.491) and elevation (r = -0.482). The multiple linear regression model explained 37% of NDVI variance (R^2 = 0.37), with the remaining 63% attributable to unmeasured factors including soil properties, terrain aspect, and land-cover heterogeneity. The strong inter-predictor correlation between elevation and precipitation (r = 0.641) indicates potential multicollinearity that warrants formal Variance Inflation Factor (VIF) assessment in future analyses.

Keywords: NDVI; forest cover change; Kurdistan Region of Iraq; dNBR; burn severity.

Introduction

Evaluating the extent of deforestation and forest degradation within countries remains a complex logistical challenge [1, 2]. In regions such as the Kurdistan Region of Iraq, the application of advanced technologies, including remote sensing and historical imagery, provides critical insights into the extent, causes, and impacts of forest degradation [3, 4]. This study examines these issues with a focus on the high-elevation central mountain forests, which have faced over four decades of challenges due to armed conflict, human displacement, and encroachment [5, 6]. Despite these pressures, evaluating changes in forest cover is further complicated by financial and safety constraints [7, 8]. By leveraging advanced methodologies, this research aims to address these barriers and provide valuable insights into the current state of regional resources, contributing to long-term environmental sustainability and improved resource management policies. Forest degradation refers to the gradual deterioration of forest ecosystems, characterized by reduced biodiversity, carbon storage, and ecological functions, often caused by human activities such as logging, mining, and agricultural expansion. Unlike deforestation, which entails the complete removal of trees, degradation leaves the forest structure partially intact but significantly reduces its ecological integrity and resilience (Sasaki and .This process affects soil quality, water cycles, and climate regulation, making it a key concern for environmental sustainability and biodiversity conservation. The Food and Agriculture Organization (FAO) highlights that forest degradation accounts for around 25% of global forest-related greenhouse gas emissions, thereby amplifying climate change risks. Examines the environmental significance of the Kurdistan region, emphasizing its rich biodiversity and ecological value. However, in recent years, the region has been increasingly threatened by deforestation and forest degradation. These challenges are driven by a combination of natural factors such as climate change and human activities, including logging, agriculture, and urban expansion. Forest degradation not only leads to biodiversity loss but also affects ecosystem services, including water regulation, carbon sequestration, and soil protection. The introduction underscores the limitations of traditional methods for monitoring forest health, which are often labor-intensive and prone to inaccuracies. In response to these [9, 10]. In the face of these challenges, the study advocates the application of advanced technologies such as remote sensing and Geographic Information Systems (GIS). These tools enable more efficient, accurate, and scalable approaches to mapping and monitoring forest degradation across large areas. The objective of evaluating forest degradation in the Kurdistan Region of Iraq using remote sensing and GIS is to monitor and quantify changes in forest cover, assess the underlying drivers of degradation, and develop actionable strategies for sustainable management. The integration of satellite imagery and GIS analysis allows for precise mapping of deforestation hotspots and provides insights into how urbanization, agricultural expansion, and climate change are impacting forest ecosystems [11, 12]. This research aims to establish a foundation for biodiversity preservation and carbon sequestration efforts while supporting policymakers in designing effective conservation initiatives. By analyzing spatial and temporal forest dynamics through metrics like the Normalized Difference Vegetation Index (NDVI) and biomass estimations, the study contributes to global climate change mitigation and sustainable land-use planning goals[11].

Materials and Methods

Study Area

The study was conducted in the Iraqi Kurdistan Region (IKR), encompassing the three governorates of Erbil (ER), Sulaimaniyah (SU), and Duhok (DU) . The IKR occupies the northern part of Iraq (Figure1), bounded by Iran to the east, Turkey to the north, and Syria to the west, and extends across approximately 50,328 km² between latitudes 34°00′10″N–37°20′33.55″N and longitudes 42°20′25.36″E–46°18′25″E [13, 14]. Erbil Governorate covers ~14,818 km² across ten administrative districts, while Duhok Governorate spans ~11,210 km² across seven districts[15]. The region is characterized by a Mediterranean-type climate cold and wet in winter, hot and dry in summer and supports diverse ecosystems, with forests and rangelands covering 6,487 km² and 8,397 km², respectively, distributed among the three governorates (ER 29%, DU 28.7%, SU 42.3%) [16, 17].Rain-fed agriculture accounts

ISSN 2072-3857

for approximately 37.2% of total agricultural land [18].

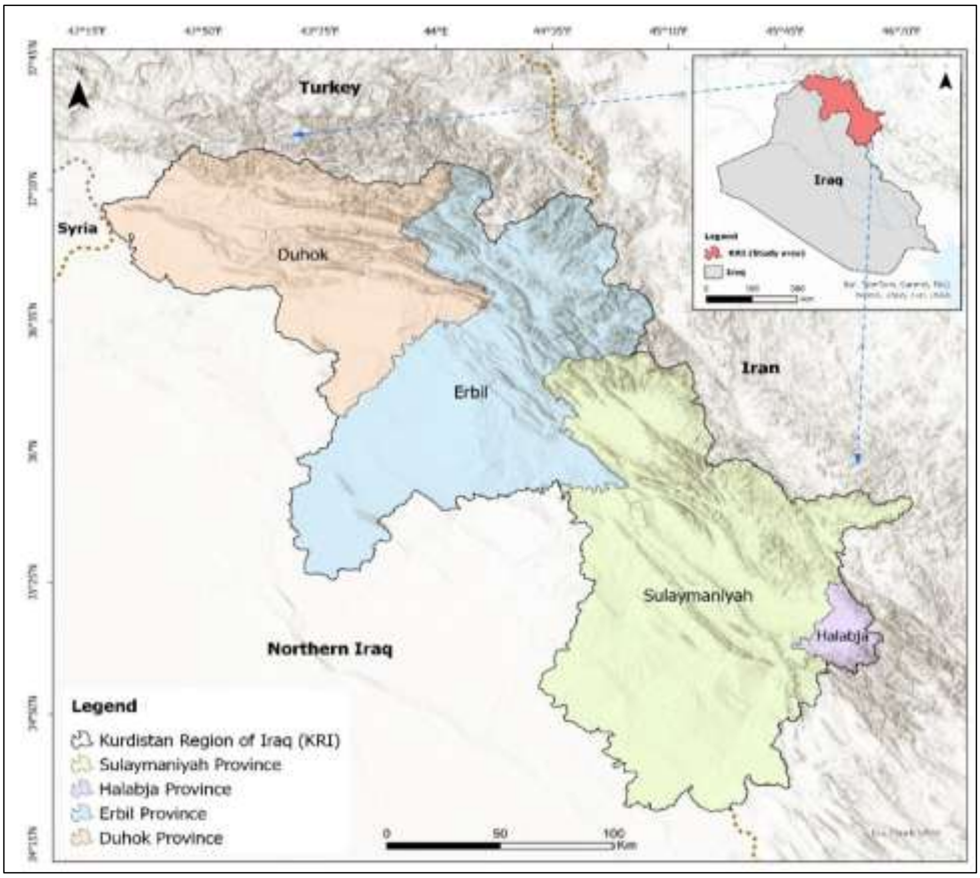

Figure 1. Study area: Kurdistan region, located in the north of Iraq.

Data Collection

Satellite Data

Sentinel-2A/B Level-1C imagery (top-of-atmosphere reflectance) was obtained from the Copernicus Open Access Hub via the Sentinel-2 Python API [22].Preprocessing was performed in Google Earth Engine (GEE) and included: (i) resampling to a standardized 10 m spatial resolution; (ii) cloud and cloud-shadow masking using the Scene Classification Layer (SCL); and (iii) BRDF correction to reduce directional reflectance artefacts associated with terrain and surface roughness [23, 24]. Processed outputs were partitioned into GeoTIFF tiles and exported for subsequent spatial analysis in QGIS (v. 24.3), including frequency distributions, cross-tabulations, and spatial autocorrelation of meteorological and remote-sensing variables [23].

Field Data

GroundTruth data were collected in collaboration with the local forestry department and included tree presence/absence records, species identification, and basic dendrometric measurements. Field checkpoints were georeferenced and overlaid with satellite-derived predictor layers (e.g., NDVI) following a spatially stratified design to minimize sampling bias and ensure adequate sample sizes for robust accuracy assessment[25, 26]. Pixel values were extracted at each checkpoint and compared

ISSN 2072-3857

with observed field conditions. Agreement between field observations and classified outputs was quantified using confusion-matrix-based metrics overall accuracy, producer's accuracy, and user's accuracy according to established map-validation protocols [27, 28].

Climate

The IKR exhibits a pronounced north–south climatic gradient, with annual precipitation ranging from ~350 mm in the southwestern lowlands to >1,200 mm in the northern and northeastern highlands [17].Based on records from 60 meteorological stations, the region is classified into three rainfall zones: assured (>500 mm), semi-assured (350–500 mm), and unassured (<350 mm)[19, 20]. The rainfall season spans October to May. Mean daily temperatures range from ~5 °C in winter to ~30 °C in summer, reaching ~50 °C in the southern plains[17]. Maximum evaporation occurs in July (~250 mm in Erbil), coinciding with peak temperatures (41.21 °C), while the coldest conditions are recorded in January in Sulaimaniyah (2.13 °C) [21].

Data Preprocessing

All multi-date imagery underwent radiometric and atmospheric correction to ensure temporal consistency. Atmospheric effects caused by aerosols and water vapour were minimized using a radiative transfer code (RTC) approach [29]. Image mosaicking and georeferencing were applied to ensure spatial continuity and accurate coordinate registration [30]. Preprocessed datasets were subsequently integrated into GIS platforms for spatial analyses, including land-use change detection, vegetation monitoring, and hydrological modelling [31].

Change Detection Analysis

LULC change was assessed using a post-classification comparison approach in ArcGIS Pro (Change Detection Wizard, Image Analyst), in which two harmonized thematic rasters (time 1 and time 2) were compared to generate class-to-class transition matrices [35-37]. Prior to analysis, all inputs were verified for radiometric and geometric consistency. For time-series analysis, a temporally normalized raster stack with cloud/shadow masks applied was used following established Landsat change.

Vegetation Indices Analysis

Vegetation dynamics were characterized using the Normalized Difference Vegetation Index (NDVI) and the Enhanced Vegetation Index (EVI), both widely applied for monitoring vegetation condition, biomass, and deforestation[43, 44]. NDVI, computed as (NIR − RED) / (NIR + RED), exploits the strong reflectance of healthy vegetation in the near-infrared and its high absorption in the red band. Values range from −1 to +1, with dense healthy canopies typically yielding 0.6–0.9, sparse or degraded vegetation approaching zero, and water bodies producing negative values[45, 46]. NDVI time series were used to track interannual.

Tools and Software

Spatial data processing and analysis were conducted using an integrated suite of GIS and remote-sensing platforms. ArcGIS Pro was used for LULC change detection, raster processing, and thematic mapping; QGIS (v. 24.3, open-source) provided complementary vector and raster analysis capabilities [47].Google Earth Engine (GEE) facilitated cloud-based, large-scale time-series analysis of Sentinel-2 imagery, substantially reducing computational overhead and enabling access to petabyte-scale geospatial datasets [24]. XLSTAT was employed for statistical analysis and land-change modelling to simulate future land-use scenarios based on historical trajectories. This multi-platform workflow ensured methodological transparency and reproducibility throughout the analysis (Figure 2).

Spectral Indices Normalized Difference Vegetation Index (NDVI)

The Normalized Difference Vegetation Index (NDVI) is among the most extensively applied spectral indices in remote sensing for assessing vegetation health, fractional cover, and phenological dynamics [45, 46]. NDVI exploits the contrasting reflectance behaviour of photosynthetically active vegetation—high reflectance in the near-infrared (NIR) and strong absorption in the red (RED) band and is calculated as:

$$\mathbf{NDVI} = (NIR - RED) / (NIR + RED) \quad \text{(Eq. 1)}$$

NDVI values range theoretically from −1 to +1. Dense, healthy vegetation typically yields values between 0.6 and 0.9, sparse or stressed vegetation falls in the range 0.2–0.5, barren or bare soils approach zero, and water bodies produce negative values [45, 48].The index is sensitive to chlorophyll content and leaf area index (LAI), making it a robust proxy for above-ground biomass and canopy greenness [49, 50]. NDVI has been extensively deployed in drought monitoring, deforestation detection, and land-cover change studies across diverse ecosystems [21, 51]. In this study, multi-temporal NDVI composites derived from Sentinel-2 imagery were used to characterize seasonal and interannual vegetation dynamics and to identify spatially coherent patterns of forest degradation across the IKR.

Statistical Analyses Bivariate (Pearson) Correlation Analysis

The strength and direction of linear relationships between drought indicators and the study variables were assessed using Pearson's product-moment correlation coefficient (r), computed in XLSTAT [52]. The coefficient ranges from −1 to +1, where the sign indicates the direction of association and the absolute value reflects its magnitude [53]. Pearson's r was calculated as:

$$\mathbf{r = [n\sum xy - (\sum x)(\sum y)] \,/\, \sqrt{\{[n\sum x^2 - (\sum x)^2][n\sum y^2 - (\sum y)^2]\}}} \quad \textbf{(Eq. 2)}$$

Where:

r = Pearson correlation coefficient

n = number of paired observations

$\sum xy$ = sum of the products of paired scores

$\sum x$, $\sum y$ = sums of the x and y scores, respectively

$\sum x^2$, $\sum y^2$ = sums of the squared x and y scores, respectively

Statistical significance was evaluated at $\alpha = 0.05$. Correlation strength was interpreted following [53] $|r| < 0.3$ (weak), 0.3–0.5 (moderate), 0.5–0.7 (strong), and >0.7 (very strong). This approach allowed systematic quantification of associations between remotely sensed vegetation indicators (e.g., NDVI) and meteorological variables (e.g., precipitation, temperature, evaporation) at the governorate and seasonal scale.

Principal Component Analysis (PCA)

Principal Component Analysis (PCA) was applied to reduce multicollinearity among environmental variables and to summarize the dominant axes of variation in the dataset [54, 55]. All variables were standardized to zero mean and unit variance prior to analysis to ensure scale invariance. The correlation matrix R of the standardized data matrix X was then decomposed via eigenanalysis:

$$\text{Where: } R = V \Lambda V^T \quad \text{(Eq. 3)}$$

R = p × p correlation matrix of standardized variables

ISSN 2072-3857

$\boldsymbol{V}$ = matrix of eigenvectors (principal component loadings)

$\boldsymbol{\Lambda}$ = diagonal matrix of eigenvalues ($\lambda_1 \geq \lambda_2 \geq \ldots \geq \lambda p$)Principal component scores for each observation were subsequently computed as:

Z = X V (Eq. 4)

Where:$\boldsymbol{Z}$ = matrix of principal component scores

$\boldsymbol{X}$ = standardized data matrix (n observations × p variables)

$\boldsymbol{V}$ = eigenvector matrix derived from R Components with eigenvalues greater than 1.0 (Kaiser criterion) were retained, and the proportion of total variance explained by each component was calculated as $\lambda_i / \sum\lambda$ [54].A scree plot was used to visually confirm the number of meaningful components. PCA biplots were generated to visualize both variable loadings and sample scores simultaneously, facilitating interpretation of the relationships between meteorological drivers and vegetation response indicators [55].

Workflow and Methodological FrameworkThe methodological framework for assessing forest degradation in the IKR integrated geospatial data acquisition, multi-temporal remote sensing analysis, field validation, and statistical modelling into a systematic, reproducible workflow. The overall procedure comprised five sequential phases (Figure 2).

Forest Classification

It is important to clarify that the term "forest" as used in this study refers to a vegetation cover class derived from a Normalized Difference Vegetation Index (NDVI) threshold, rather than a formal forest inventory definition. Conventional forestry definitions, such as that of the Food and Agriculture Organization (FAO, 2020), require canopy cover ≥10%, a minimum tree height of 5 m at maturity, and a minimum mapping unit of 0.5 ha. Because such structural parameters cannot be directly retrieved from medium-resolution optical imagery alone, our classification should be interpreted as a vegetation greenness proxy that approximates, but does not strictly equal, forest cover. To narrow this gap, the operational definition adopted in the revised analysis enforces the FAO 0.5 ha minimum patch size and a multi-year persistence rule (≥3 consecutive years above the NDVI threshold) before a pixel is reported as "forest."

ISSN 2072-3857

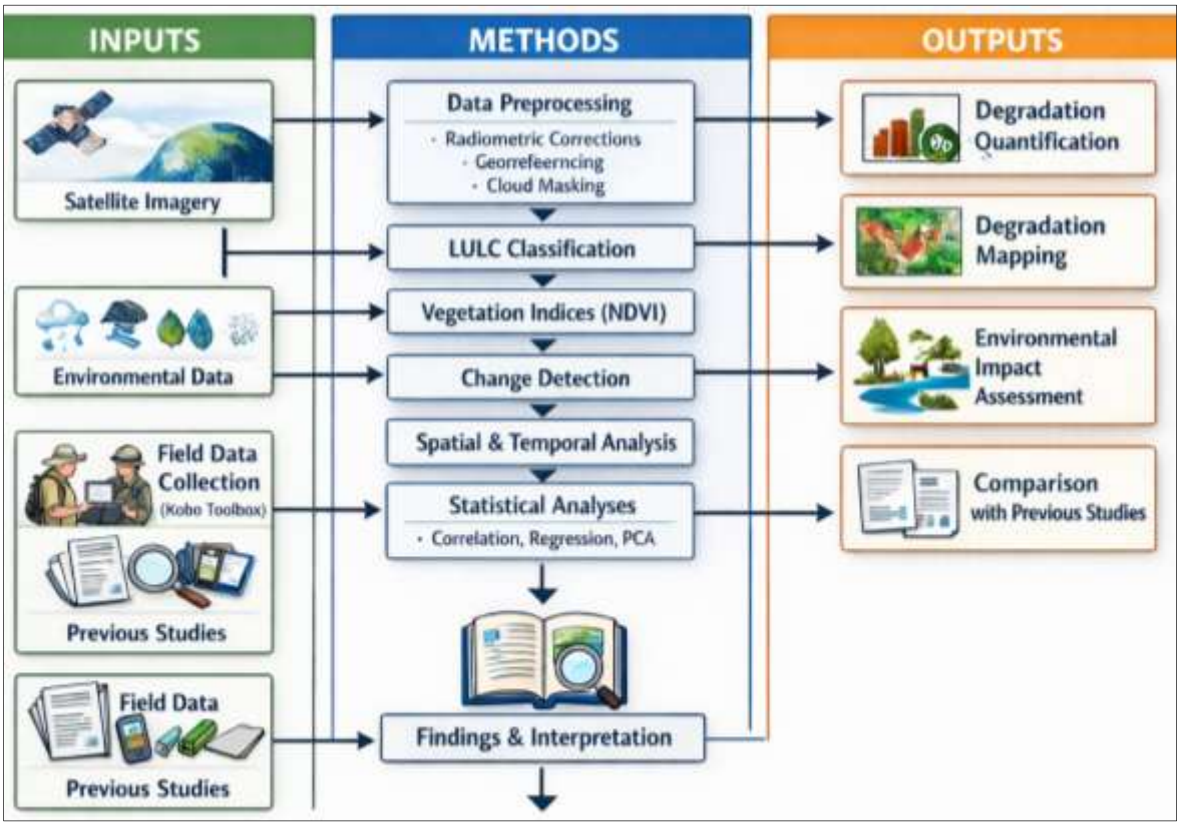

Fig 2. Flowchart or Diagram Representing the Analysis Procedure

RESULTS AND DISCUSSION

Forest and Non-Forest Land Cover in Kurdistan Region Governorate,2016-2024)

Figures 3 and 4 present the annual NDVI-derived forest/non-forest classification and the corresponding year-to-year change maps for the Kurdistan Region between 2016 and 2024. NDVI was selected as the primary classification index owing to its well-established sensitivity to vegetation greenness, derived from the spectral contrast between near-infrared and red reflectance, and its broad application in regional vegetation monitoring [56, 57]. In spatial terms, both figures consistently indicate that forested areas are concentrated in the northern and northeastern mountainous zones of the Kurdistan Region, while the central and southern plains remain predominantly non-forest throughout the study period. This distribution is broadly consistent with the region's topographic and climatic gradients, whereby higher elevations generally support denser natural vegetation than the lowland plains.Table 4.1 quantifies these patterns and reveals substantial interannual variability in the NDVI-derived forest class. Forest cover ranged from 18.0% (8,401.0 km²) in 2022 to 25.2% (11,797.2 km²) in 2019, against a constant study area of approximately 46,781 km². Over the full study period, forest extent increased from 8,970.9 km² (19.2%) in 2016 to 10,471.2 km² (22.4%) in 2024, representing a net gain of approximately 1,500 km² (+3.2 percentage points). The change maps (Figure 3) highlight two particularly notable phases. Forest extent expanded markedly between 2018 and 2019, corresponding to the largest single-year increase in the time series (+2,144.2 km²). This expansion was followed by a sustained contraction from 2019 through 2022, with the sharpest decline occurring between 2020 and 2021 (−1,981.2 km²).

ISSN 2072-3857

Forest cover subsequently rebounded in 2023 (+2,127.8 km²) before remaining broadly stable into 2024 (−57.6 km²).

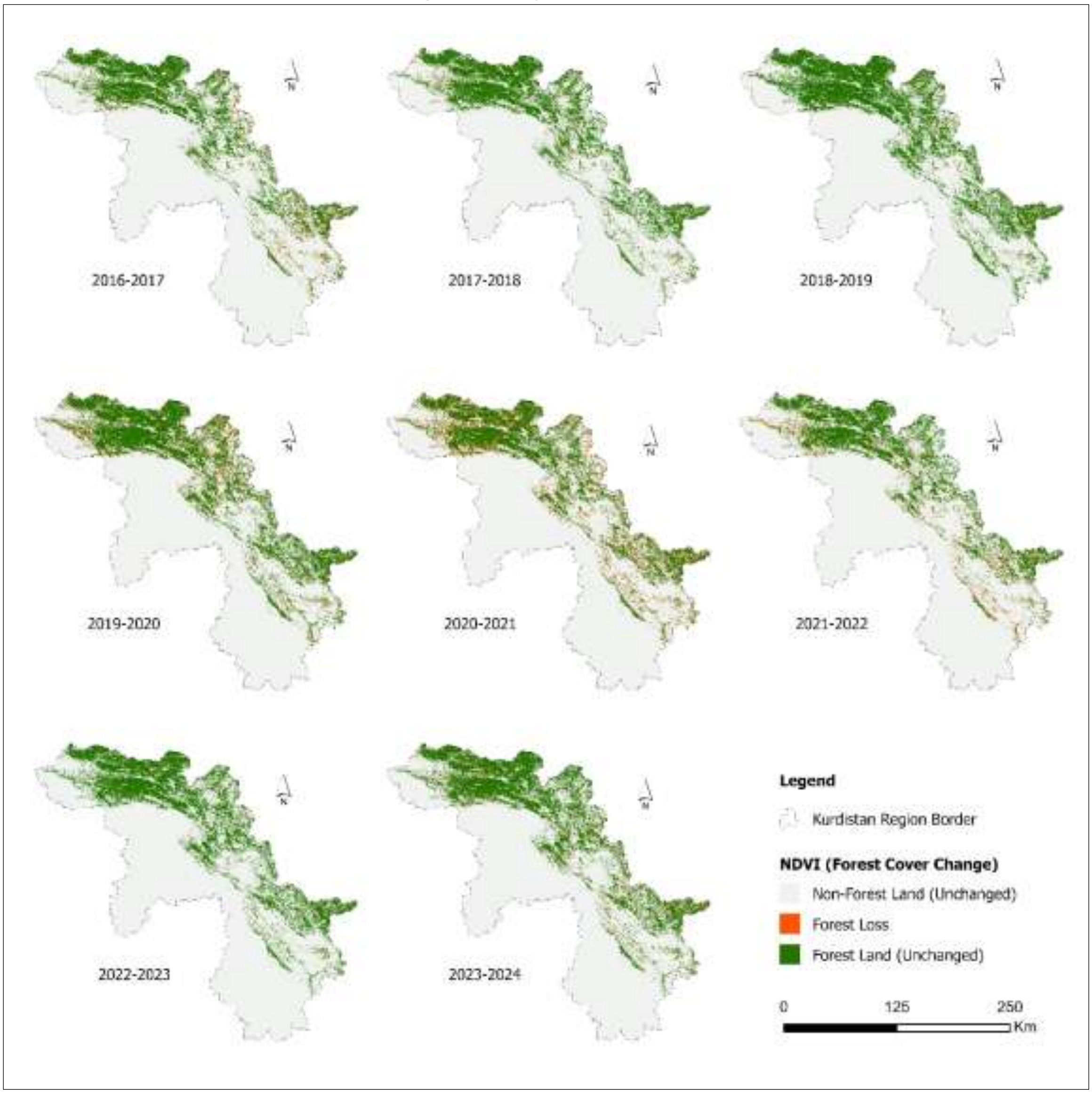

Fig 3. Annual Forest Cover Change in the Kurdistan Region of Iraq (2016–2024)

These fluctuations suggest that year-to-year changes in the NDVI-derived forest signal reflect a combination of genuine land-cover dynamics and shifts in vegetation vigor tied to climate variability, rather than structural deforestation or afforestation alone. It is important to note that the term 'forest' here refers to an NDVI-based forestland class, not a formal inventory definition. Conventional forest definitions typically incorporate canopy cover thresholds, minimum tree height, land use, and minimum mapping unit requirements criteria that NDVI alone cannot fully satisfy [58]. Furthermore, NDVI is susceptible to phenological variation, rainfall-driven greenness changes, soil background reflectance, and saturation effects in high-biomass conditions. To align the classification with internationally recognised standards, future work should adopt the FAO Global Forest Resources Assessment definition, which requires a minimum canopy cover of 10%, a minimum area of 0.5 ha, and a potential tree height of at least 5 m criteria that a spectral threshold alone cannot

ISSN 2072-3857

fully verify. Such alignment would enable distinction between permanent land-cover conversion (structural deforestation) and temporary climatic greening driven by interannual precipitation variability [59, 60]. To facilitate defensible area change reporting, future analyses should adopt a formal accuracy and change-map validation framework, incorporating sample-based reference data, error matrices, and area-adjusted accuracy estimates methodological standards that are essential for minimising area estimation bias in land cover and land change studies [61, 62].

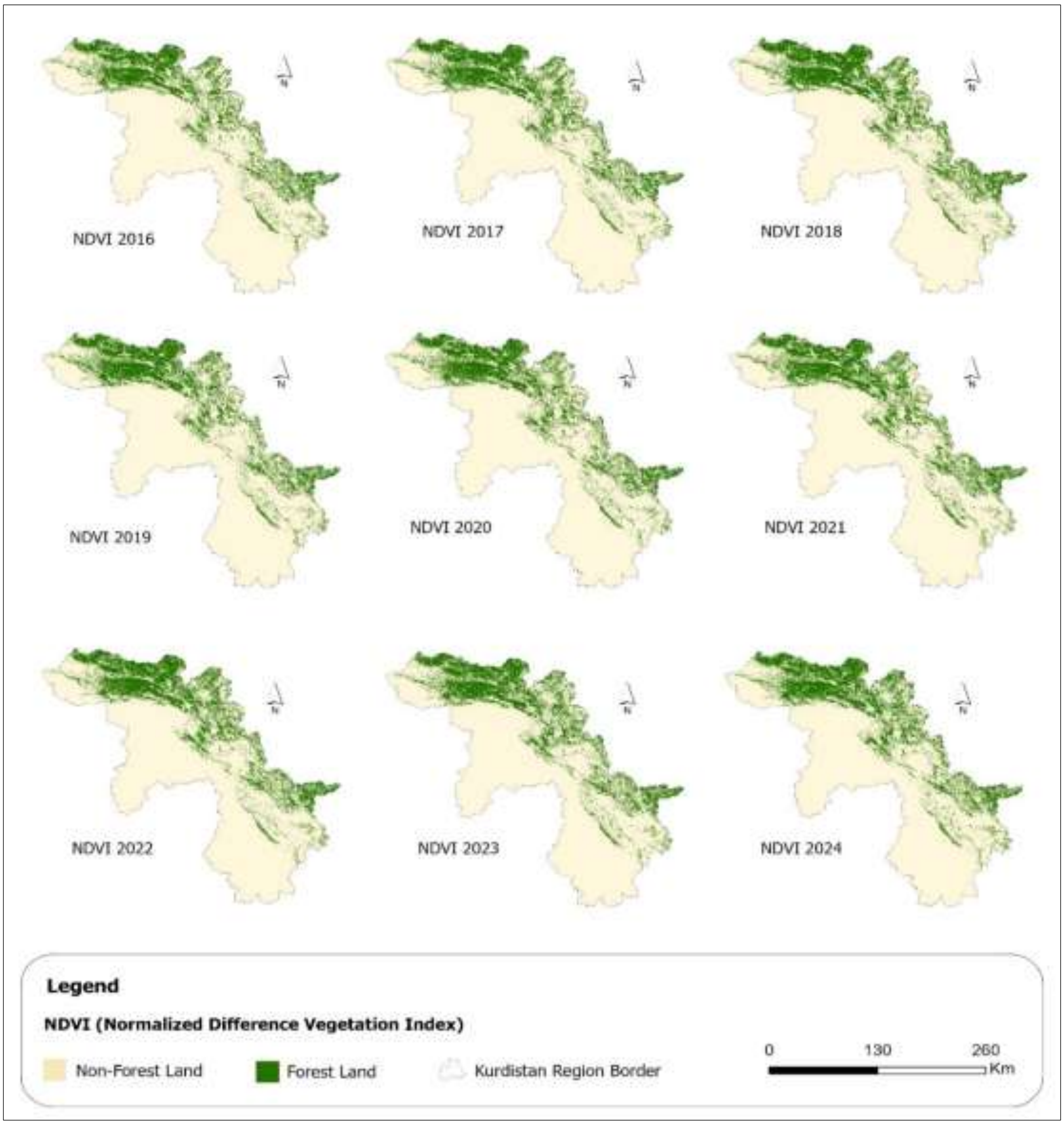

Fig 4. Annual NDVI-Based Forest Land Classification in the Kurdistan Region of Iraq (2016–2024).

ISSN 2072-3857

Table 1. Annual Forest and Non-Forest Land Cover Statistics in the Kurdistan Region of Iraq (2016–2024)

Years	Non-Forest Land		Forest Land		SUM	
	Area_km^2	%	Area_km^2	%	Area_km^2	%
2016	37810.1	80.8	8970.9	19.2	46781	100
2017	37889.7	81.0	8891.2	19.0	46781	100
2018	37128.0	79.4	9653.0	20.6	46781	100
2019	34983.7	74.8	11797.2	25.2	46781	100
2020	35888.5	76.7	10892.5	23.3	46781	100
2021	37869.7	81.0	8911.3	19.0	46781	100
2022	38379.9	82.0	8401.0	18.0	46781	100
2023	36252.2	77.5	10528.8	22.5	46781	100
2024	36309.8	77.6	10471.2	22.4	46781	100

Annual Percentage of Forest and Non-Forest Land Cover in Halabja Governorate districts, 2016–2024

Figure 5 and Table 2 summarise the annual NDVI-derived forest/non-forest cover for Halabja Governorate, whose total area remains approximately 889 km² throughout the study period. Non-forest land consistently dominated, ranging between 79.1% (703.3 km²) in 2019 and 88.2% (784.5 km²) in 2022. Forest cover correspondingly varied from a minimum of 11.8% (104.7 km²) in 2022 to a maximum of 20.9% (185.9 km²) in 2019.[56, 57] .A pronounced short-term expansion is evident from 2018 to 2019, when forest area increased from 122.6 km² (13.8%) to 185.9 km² (20.9%), the highest proportion recorded in the time series. The partial retreat in 2020 to 167.4 km² (18.8%) suggests that the 2019 peak may partly reflect an exceptionally favourable growing season characterised by heightened vegetation greenness, rather than a permanent structural shift in land cover. From 2020 to 2022, the forest class contracted progressively to its minimum value of 104.7 km² (11.8%). This period likely reflects climatically induced reductions in vegetation greenness potentially associated with drought or heat stress, differences in imagery acquisition timing, or disturbance events which would shift pixels below the NDVI threshold used to delineate the forest class even where substantial tree cover persisted. Such threshold sensitivity is a recognised limitation of single-index NDVI classification, as the index responds to canopy health, moisture conditions, phenological stage, and soil background, meaning that apparent forest loss may in some cases indicate vegetation degradation or reduced vigour rather than complete conversion to non-forest [60] .Following the 2022 minimum, forest cover rebounded to 160.3 km² (18.0%) in 2023 before declining marginally to 152.0 km² (17.1%) in 2024. Despite the pronounced interannual variability, net change across the full period was modest: forest increased by approximately 1.9 km² (+0.2 percentage points) between 2016 and 2024. This pattern indicates that interannual variability constitutes the dominant signal in Halabja's NDVI-derived forest record, and that short-term gain/loss estimates should be interpreted with caution unless supported by consistent seasonal composites and independent reference data. To improve confidence in reported changes, best practice recommends (i) applying a consistent seasonal compositing window each year, or

ISSN 2072-3857

using multi-date composites to reduce phenological bias; (ii) [61, 62].

Table 2. Annual Forest and Non-Forest Land Cover Statistics in Halabja Governorate (2016–2024

Years	Non-Forest Land			Forest Land			SUM	
	count	Area_km^2	%	count	Area_km^2	%	Area_km^2	%
2016	7390541	739.1	83.1	1500792	150.1	16.9	889	100
2017	7623618	762.4	85.8	1267715	126.8	14.3	889	100
2018	7665575	766.6	86.2	1225758	122.6	13.8	889	100
2019	7032800	703.3	79.1	1858533	185.9	20.9	889	100
2020	7217687	721.8	81.2	1673646	167.4	18.8	889	100
2021	7776488	777.6	87.5	1114845	111.5	12.5	889	100
2022	7844682	784.5	88.2	1046651	104.7	11.8	889	100
2023	7288071	728.8	82.0	1603262	160.3	18.0	889	100
2024	7370970	737.1	82.9	1520363	152.0	17.1	889	100

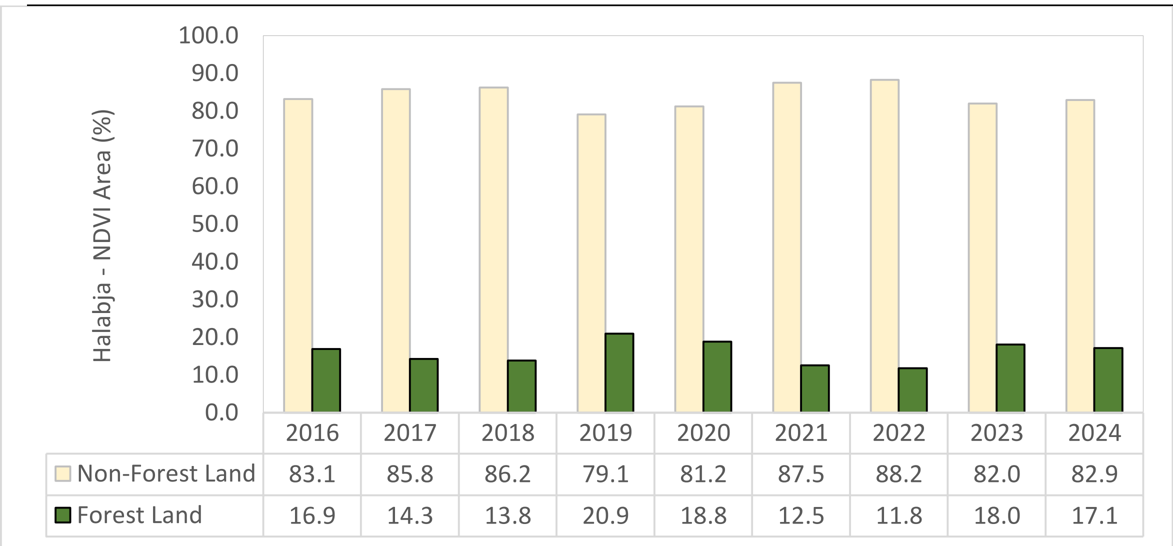

Fig 5. Forest/Non-Forest Distribution and Precipitation Relationships, 2016–2024

Figure 6 summarizes the annual proportion of forest and non-forest land derived from the NDVI-based classification (threshold = 0.2) across the Kurdistan Region as a whole. Non-forest land dominates throughout the period, ranging from 74.8% to 82.0%, while forest cover varies between 18.0% and 25.2%. Three broad phases are discernible in the time series. Between 2016 and 2018, forest cover remains relatively stable (approximately 19.0–20.6%), indicating limited year-to-year variability. A marked expansion follows in 2019, when forestland reaches its maximum proportion (25.2%) and non-forest drops to its minimum (74.8%). After 2019, forest cover declines steadily, reaching a minimum of 18.0% in 2022, before recovering in 2023–2024 to approximately 22.4–22.5%.

ISSN 2072-3857

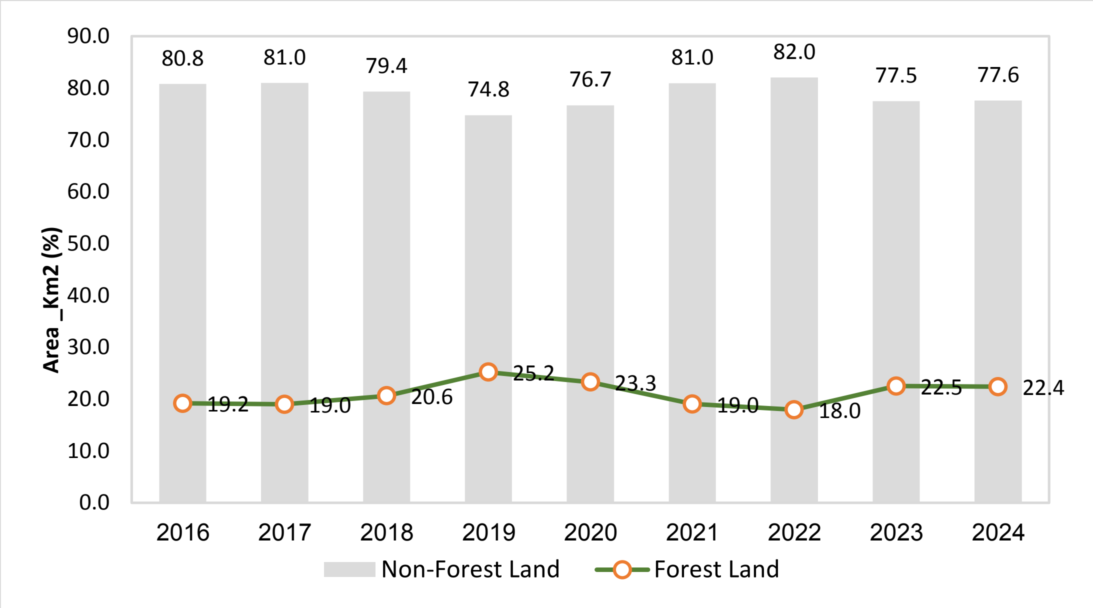

Fig 6. Forest And Non-Forest Land Area Distribution (2016 – 2024)

This peak, decline, and recovery pattern often reflects not only land-cover conversion but also interannual variation in vegetation vigor driven by moisture availability, phenology, and the seasonal timing of imagery [60].The classes are derived from NDVI; changes should be interpreted carefully: NDVI can be influenced by soil background, atmospheric effects, and saturation in dense vegetation. [59]. Finally, reporting forest/non-forest trends is strongest when accompanied by an accuracy assessment using reference samples and an error matrix, especially if results are used for policy or area-change conclusions[61, 62].

Table 3. KRI Land Cover Changes and Precipitation by Year Interval (2016-2024)

Years	**Non-Forest Land**	**Forest Loss**	**Forest Land**	**Precipitation**
2016-2017	79.2	2.0	18.8	501.1
2017-2018	78.2	1.2	20.7	614.2
2018-2019	74.0	0.8	25.2	1169.8
2019-2020	73.7	3.0	23.3	731.8
2020-2021	75.9	5.0	19.1	372.2
2021-2022	79.3	2.8	18.0	449.0
2022-2023	77.0	0.5	22.5	580.7
2023-2024	75.9	1.7	22.4	910.6

ISSN 2072-3857

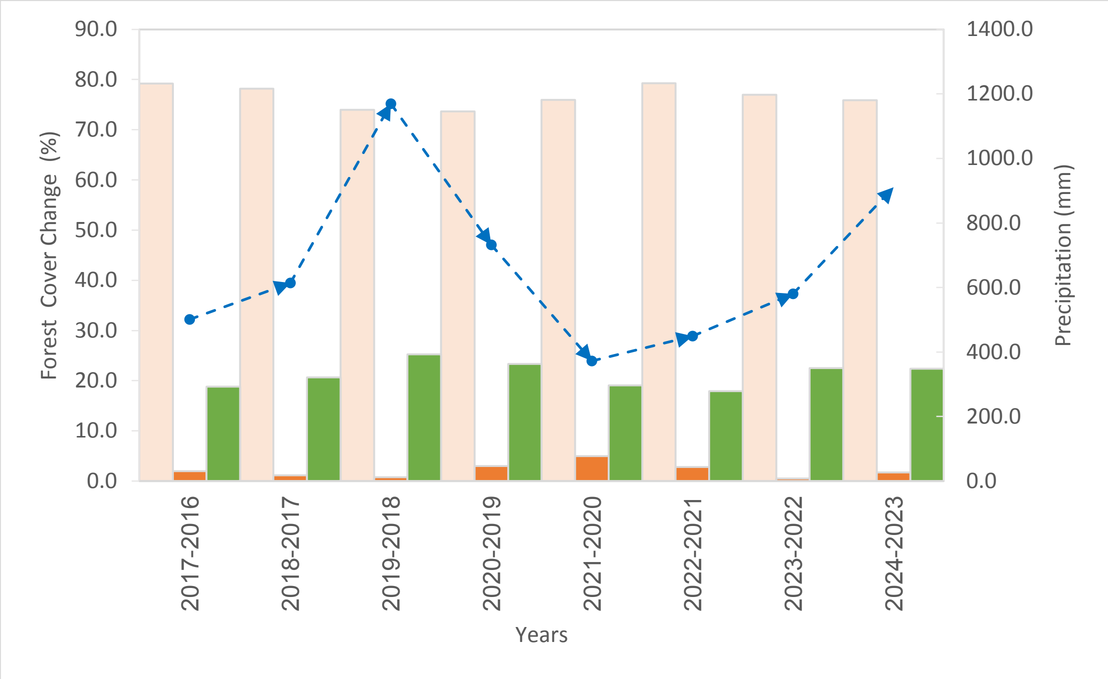

Fig 7. Forest Cover Change (%) and Precipitation (mm)

Figure 7 and Table 3 place these dynamics in the context of annual-interval precipitation data for the Kurdistan Region. A clear wet-year response is evident in 2018–2019, which recorded the highest precipitation (1,169.8 mm) and coincided with the maximum forest proportion (25.2%), the lowest non-forest share (74.0%), and the lowest forest loss rate (0.8%). This pattern is consistent with the well-documented positive relationship between rainfall and vegetation greenness in semi-arid to mountainous Mediterranean-type environments, where NDVI is strongly responsive to moisture availability. In contrast, the driest interval 2020–2021, with only 372.2 mm recorded coincided with the most pronounced degradation signal: forest loss peaked at 5.0% and forest land declined to 19.1%. The following interval (2021–2022, 449.0 mm) continued to show elevated forest loss (2.8%) and reduced forest land (18.0%). These results suggest that moisture stress during dry years likely suppresses vegetation greenness sufficiently to shift pixels below the NDVI classification threshold, generating apparent forest loss that may not correspond entirely to physical tree removal or land-cover conversion.The subsequent recovery from 2022–2023 onward (precipitation increasing to 580.7 mm then 910.6 mm) coincides with a return of forest proportions to approximately 22–23% and declining loss rates, lending further support to a climate-driven interpretation of much of the interannual variability [56, 63].Land management activities, fire disturbance, grazing pressure, pest outbreaks, and land-use expansion can each independently affect forest condition and land-cover transitions. The precipitation–forest relationship documented here is therefore best interpreted as an important climatic modulation of NDVI-derived forest signals, rather than a single-cause explanation for observed changes. Table 4 decomposes NDVI-based forest dynamics into three transition components for each annual interval: NFL→FL (apparent gain), FL→NFL (apparent loss), and Stable FL (persistence). This gross change accounting framework is recommended in land-change studies because it distinguishes gain, loss, and stable areas rather than masking important dynamics within a net change statistic [57, 63].Across all intervals, NFL→FL occupies the largest share of the landscape (approximately 73.7–79.3%), consistent with most of the region remaining persistently non-forest. FL→NFL represents the smallest component (approximately 0.8–5.3%), while Stable FL exhibits the strongest temporal variability (approximately 16.3–22.2%). The interval 2018–2019 shows the strongest apparent gain signal (NFL→FL = 2,503.1 km², 5.3%; FL→NFL = 358.9 km², 0.8%), consistent with the wet-year conditions prevailing during this period [46]. Conversely, 2020–2021 records the most pronounced apparent loss (FL→NFL = 2,343.0 km², 5.0%; NFL→FL = 360.7 km², 0.8%), consistent with moisture stress during the driest interval in the record. A second notable gain phase emerges in 2022–2023 (NFL→FL = 2,358.4 km², 5.0%; FL→NFL = 230.6 km², 0.5%), indicating a broad recovery of forest-class pixels following improved moisture conditions. As these transitions are derived from an NDVI-based classification, NFL→FL may represent either genuine forest recovery or an improvement in vegetation vigour that raises NDVI above the classification threshold; similarly, FL→NFL may reflect forest degradation or phenological and seasonal effects rather than permanent cover removal. For this reason, change dynamics are most reliably interpreted alongside consistent seasonal compositing, supplementary spectral indices, and reference-data validation following established accuracy and area estimation guidelines [57].Table 4 decomposes NDVI-based forest dynamics into three components for each year interval: (i) NFL→FL (areas that became forest), (ii) FL→NFL (areas that shifted from forest to non-forest), and (iii) Stable FL (areas that remained forest). This type of from–to change accounting is commonly used in land-change studies because it distinguishes between gross gains, gross losses, and persistence, rather than reporting only net change[64].

Across all intervals, NFL→FL accounts for the largest share of the landscape (≈73.7–79.3%), reflecting that most of the region remains persistently non-forest and many areas remain in the non-forest class. The smallest component is typically FL→NFL (≈0.8–5.3%), representing mapped forest loss or decline below the NDVI threshold. Stable FL varies more strongly over time (≈16.3–22.2%), indicating that forest persistence fluctuated across intervals consistent with the temporal variability observed in earlier figures and tables. The 2018–2019 interval shows the strongest "gain" signal: NFL→FL reaches 2,503.1 km² (5.3%), while FL→NFL is only 358.9 km² (0.8%), and Stable FL increases to 9,311.1 km² (19.9%). This suggests that forest persistence and apparent expansion were highest during this interval, aligning with the wet-year conditions previously shown (high precipitation in 2018–2019) and the known sensitivity of NDVI-derived vegetation classes to moisture-driven greenness [46]. In contrast, the interval 2020–2021 reflects the most pronounced "loss" period: FL→NFL rises to 2,343.0 km² (5.0%), while NFL→FL falls to 360.7 km² (0.8%), and Stable FL declines to 8,563.6 km² (18.3%). This pattern indicates a net shift away from the forest class, which is consistent with the low-precipitation interval, highlighted previously and suggests climate-driven stress, disturbance, or both. A second notable gain interval occurs in 2022–2023, where NFL→FL again becomes high (2,358.4 km²; 5.0%) while FL→NFL is minimal (230.6 km²; 0.5%), and Stable FL remains moderate (8,187.5 km²; 17.5%). This indicates a broad recovery of forest-class pixels during 2022–2023, consistent with improved moisture conditions and vegetation vigor in that period. It is important to note that because these transitions are derived from an NDVI-based forest/non-forest classification, NFL→FL may represent either true forest recovery/afforestation or improvement in

ISSN 2072-3857

vegetation vigor that raises NDVI above the threshold; similarly, FL→NFL may represent forest degradation or seasonal/phenological effects rather than complete forest removal.

Table 4. Land Cover Change Percentages (Non-Forest Land, Forest Loss, and Forest Land) by Year Interval

Year	Non-Forest Land	Forest Loss	Forest Land
2016-2017	82.2	4.2	13.6
2017-2018	83.6	2.7	13.8
2018-2019	78.0	1.1	20.9
2019-2020	76.9	4.2	18.8
2020-2021	80.1	7.4	12.5
2021-2022	84.9	3.4	11.8
2022-2023	81.0	1.0	18.0
2023-2024	80.1	2.8	17.1

Across all year-intervals (2016–2017 to 2023–2024), Non-Forest Land dominates the landscape, ranging from 76.9% to 84.9%. Forest-related classes remain comparatively small, with Forest Land between 11.8% and 20.9%, while Forest Loss varies from 1.0% to 7.4%. This indicates that the study area is largely non-forested, and annual forest dynamics occur within a limited proportion of the total land cover.

Forest Fire Disturbance Severity Kurdistan Region, 2016–2024

Figure 8, and Figure 9 summarises cumulative dNBR-derived burn severity classes across the Kurdistan Region for 2016–2024. At the regional scale, the vast majority of land (approximately 45,005.4 km²) falls in the no-burn/low-severity class, with medium severity accounting for approximately 1,507.7 km² (3.22%) and high severity for approximately 267.0 km² (0.57%). While severe vegetation disturbance is therefore limited in spatial extent, it is strongly concentrated in a subset of northern and northeastern districts. Medium-severity disturbance is most heavily concentrated in Amedi (245.6 km², 16.3% of the regional medium-severity total), Soran (219.0 km², 14.5%), Pshdar (156.0 km², 10.3%), Penjwen (103.6 km², 6.9%), and Choman (85.5 km², 5.7%) five districts that together account for approximately 54% of the regional medium-severity area, confirming a clear hotspot pattern rather than a uniform regional distribution.High-severity disturbance is even more spatially clustered. Amedi alone accounts for 53.9 km² (20.2%) of the regional high-severity area, with Bardarash (31.3 km², 11.7%), Soran (28.3 km², 10.6%), Pshdar (26.0 km², 9.8%), and Shekhan (24.9 km², 9.3%) as the next largest contributors. These five districts collectively represent approximately 62% of all high-severity disturbance. Figures 4.6 and 4.7 visually confirm this spatial pattern, showing that the highest severity classes cluster along the mountainous northern and eastern belt of the Kurdistan Region, particularly around the Amedi, Soran, Pshdar, and Penjwen corridor.

ISSN 2072-3857

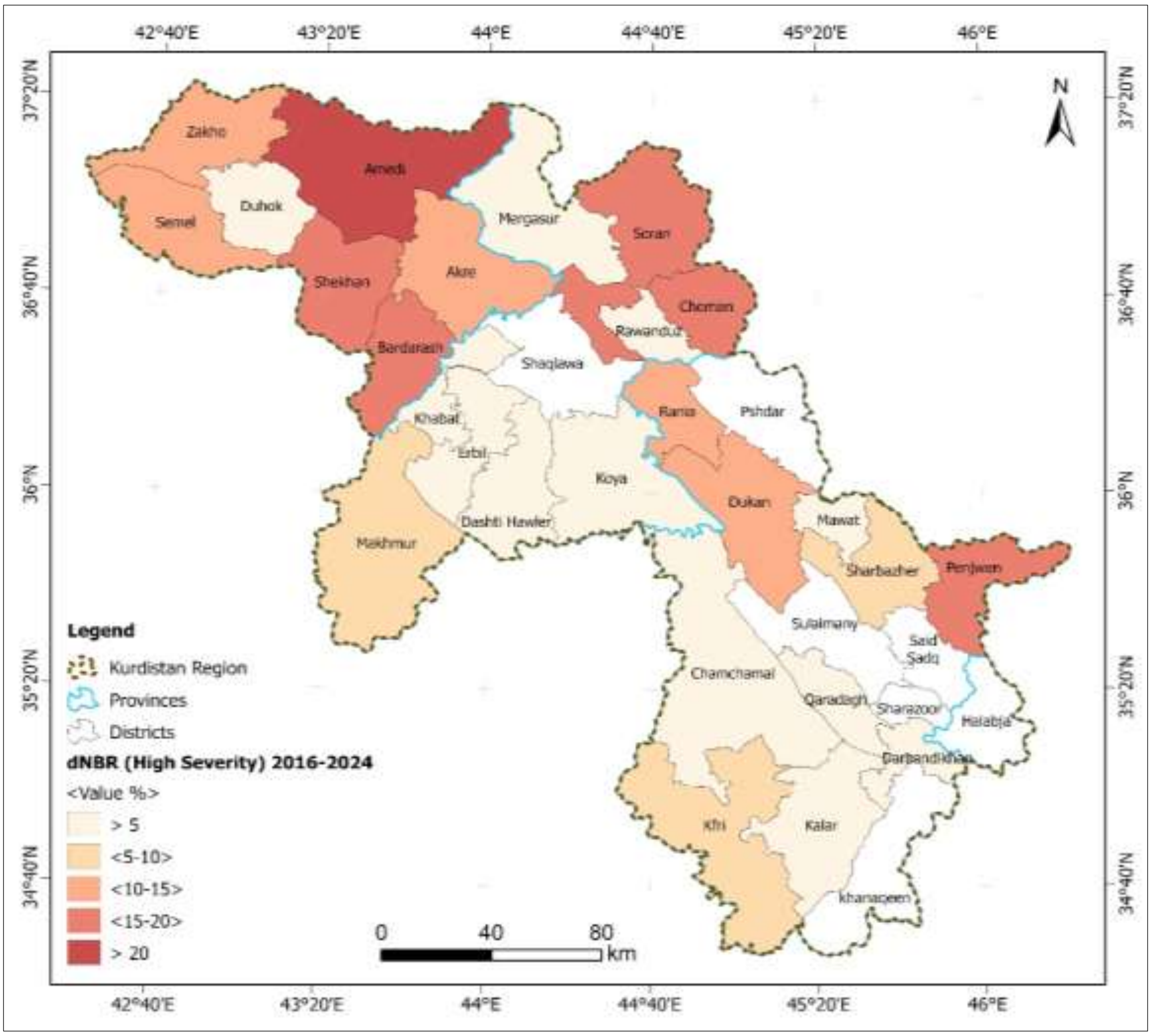

Fig 8. dNBR(Differenced Normalized Burn Ratio) indicating high areas with the most intense forest disturbance or vegetation loss in the Kurdistan Region of Iraq between 2016 – 2024

The concentration of medium and high dNBR in these districts is ecologically consistent with their landscape context: they encompass mountain forests on steep slopes with continuous vegetation conditions that favour both the occurrence of intense burning and the detection of strong post-fire spectral differences by remote sensing. In contrast, districts dominated by urban land, agriculture, or sparse vegetation show negligible high-severity values, as lower biomass density and non-forested surfaces produce weak disturbance signals.

ISSN 2072-3857

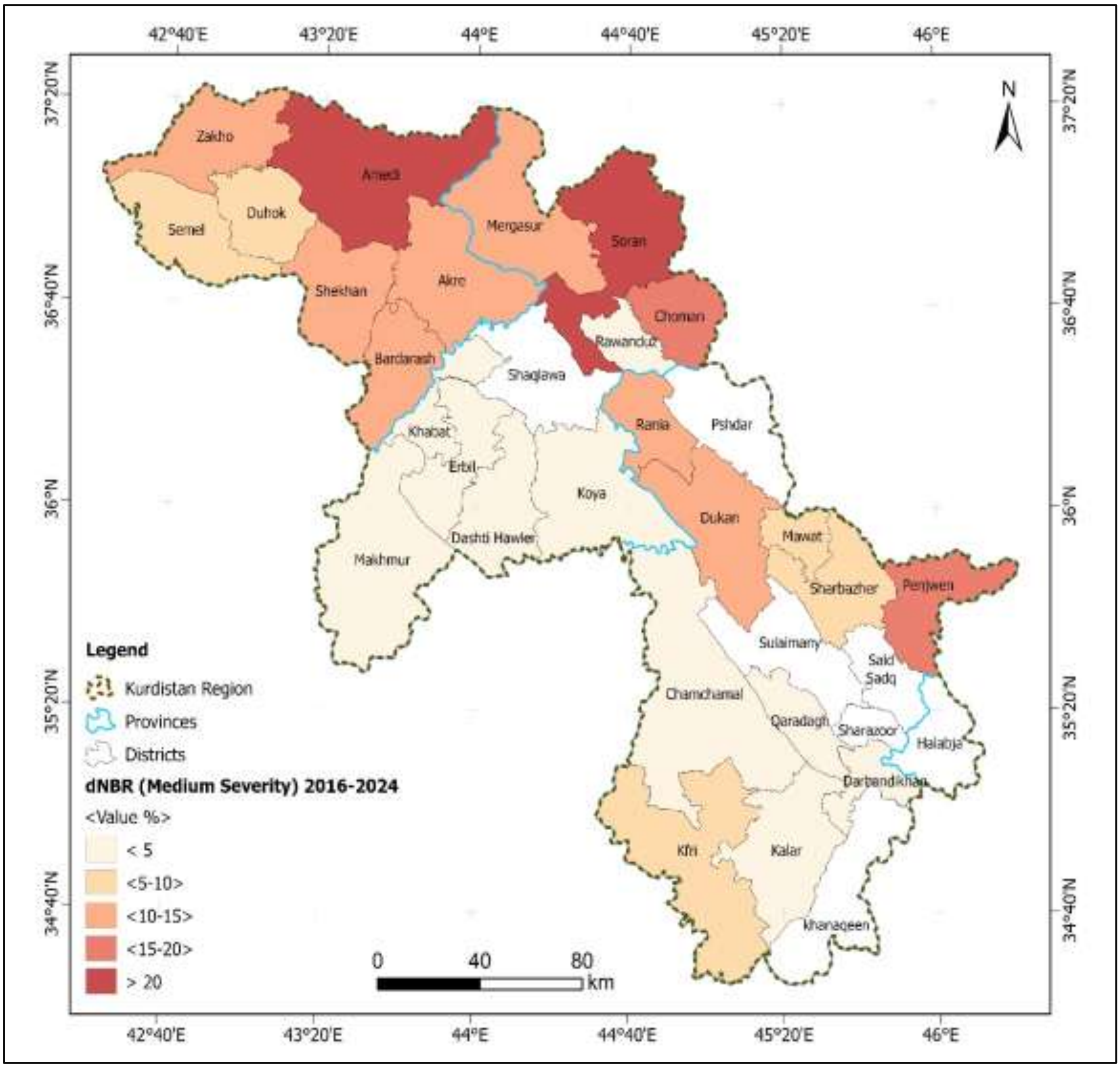

Fig 9. dNBR(Differenced Normalized Burn Ratio) indicating medium severity forest disturbance or degradation in the Kurdistan Region of Iraq between 2016 – 2024.

The fact that high severity remains far smaller than medium severity (approximately 267 km² versus 1,508 km²) suggests that most disturbance over the period constitutes moderate degradation rather than complete canopy removal, though high-severity patches in the core hotspot areas can drive disproportionate impacts including loss of forest structure, erosion risk, and reduced regeneration potential particularly on steep terrain where post-fire soil exposure is critical.Since these maps aggregate disturbance across 2016–2024, hotspot districts should be treated as priority zones for ongoing monitoring and targeted management rather than as reflecting a single fire event. The interpretation is most robust when combined with annual fire occurrence records, climate anomaly data, and field observations to determine whether hotspots are driven by repeated fire events, drought-stressed vegetation, anthropogenic land-use pressure, or some combination thereof.

Statistical Analysis Results

Pearson correlation analysis of 355 in Table 8 observations revealed several statistically significant relationships among topographic, climatic, and vegetation

ISSN 2072-3857

variables, indicating a coherent environmental structure across the IKR study area. The strongest positive association was observed between DEM and precipitation ($r = 0.641$, $p < 0.05$), suggesting that higher-elevation areas receive greater rainfall. This pattern is consistent with orographic precipitation processes, in which rising air masses cool and condense over elevated terrain, enhancing precipitation at altitude [65, 66]. A comparably strong positive correlation between DEM and slope ($r = 0.632$, $p < 0.05$) was likewise anticipated, as mountainous landscapes typically combine higher elevations with steeper gradients arising from tectonic uplift, channel incision, and long-term geomorphic evolution [67]. The correlation matrix further demonstrated that NDVI was positively associated with precipitation ($r = 0.540$, $p < 0.05$), indicating that vegetation greenness is enhanced in areas of greater water availability. This finding is consistent with a substantial body of ecological and remote-sensing research demonstrating precipitation as a primary control on vegetation productivity and canopy development, particularly in water-limited and seasonally dry environments [68-70].The positive NDVI , and precipitation relationship documented here therefore supports moisture availability as a central driver of vegetation condition across the sampled landscape. Several negative correlations reflected expected environmental constraints. Temperature was negatively correlated with precipitation ($r = -0.491$, $p < 0.05$), consistent with the tendency for warmer zones to be drier under the hydroclimatic gradients and atmospheric circulation patterns documented for the broader region [71]. Temperature also showed a negative correlation with DEM ($r = -0.482$, $p < 0.05$), consistent with the well-established environmental lapse rate, whereby air temperature decreases with increasing elevation [72]. Together, these relationships indicate that elevation exerts both direct and indirect influences on vegetation, operating through its control on temperature and precipitation regimes simultaneously.

ISSN 2072-3857

Table 8. Pearson Correlation Matrix of Environmental Variables and Vegetation Index for IKR

Correlation matrix (Pearson): IKR

Variables	NDVI	Burn	DEM	Humidity	Precipitation(mm)	Slope	Temperature
NDVI	**1**	**0.153**	**0.509**	**-0.249**	**0.540**	**0.403**	**-0.364**
Burn	**0.153**	**1**	**0.446**	**-0.122**	**0.337**	**0.129**	**-0.338**
DEM(M)	**0.509**	**0.446**	**1**	**-0.112**	**0.641**	**0.632**	**-0.482**
Humidity%	**-0.249**	**-0.122**	**-0.112**	**1**	**-0.349**	**-0.176**	-0.019
Precipitation(mm)	**0.540**	**0.337**	**0.641**	**-0.349**	**1**	**0.488**	**-0.491**
Slope	**0.403**	**0.129**	**0.632**	**-0.176**	**0.488**	**1**	**-0.293**
Temperature(C)	**-0.364**	**-0.338**	**-0.482**	-0.019	**-0.491**	**-0.293**	**1**

*Values in bold are different from 0 with a significance level **alpha=0.05***

Multiple Regression Analysis Results IKR

For the IKR dataset (n = 355; DF = 347), the multiple linear regression model in Table 9, 10 and Figure 10 demonstrates a moderate overall fit for NDVI prediction. The model explains 37% of NDVI variance ($R^2 = 0.37$; Adjusted $R^2 = 0.36$), and the close correspondence between these two statistics confirms that explanatory power is not artificially inflated by an excessive number of predictors. Relative to governorate-level models, the higher R^2 at the regional scale reflects the broader environmental gradients captured when observations span the full climate–topography–vegetation range of the IKR, allowing environmental predictors to account for a larger share of NDVI variability.Error metrics indicate reasonable predictive accuracy given the spatial complexity of NDVI across this heterogeneous landscape. The MSE of 0.01 and RMSE of 0.08 imply a typical prediction error of approximately 0.08 NDVI units. The MAPE of 41.03% is comparatively high, which is a well-recognised artefact of applying percentage-based error metrics to NDVI datasets that include low or near-zero values in sparse-vegetation and bare-soil areas, where small absolute errors translate into large relative errors. The Durbin–Watson statistic (DW = 1.89) is close to 2, indicating that residual autocorrelation is likely weak, supporting the assumption of independence more strongly than is common in environmental regressions. Model selection statistics (Cp = 8.0; AIC = −1765.25; SBC = −1734.27) suggest an acceptable model structure relative to alternatives assessed within the same framework, and the reported PC = 0.66 is consistent with the moderate R^2 and RMSE values.The fitted regression equation is:

$$NDVI = 0.678 - 0.043(Burn) + 6.54 \times 10^{-5}(DEM) - 0.006(Humidity) + 1.08 \times 10^{-4}(Precipitation) - 0.017(Temperature).$$

Among the predictors, DEM emerged as a strong positive driver ($t = 5.373$, $p < 0.0001$), indicating that higher elevations are associated with more productive vegetation. This is consistent with mountain ecology research demonstrating that many montane vegetation systems benefit from cooler conditions and improved moisture balance at moderate to higher elevations [73, 74]. Precipitation also exerted a significant positive effect on NDVI ($t = 4.289$, $p < 0.0001$), further confirming water availability as a central control on vegetation productivity and greenness [68,

ISSN 2072-3857

70]. The model identified a significant negative effect of burn severity on NDVI ($t = -2.933$, $p = 0.004$), indicating that vegetation greenness declines in areas experiencing more intense burning even after controlling for other environmental factors. This finding is in agreement with fire ecology principles and empirical studies demonstrating that higher fire severity can reduce canopy cover, delay post-fire regrowth, and impair vegetation recovery [75-77]. The persistence of a significant burn effect within the multivariate model confirms that fire disturbance independently affects vegetation health beyond the combined influence of elevation and climate. Temperature showed a significant negative relationship with NDVI ($t = -2.431$, $p = 0.016$), indicating that warmer conditions are associated with reduced vegetation greenness. This is consistent with research demonstrating that elevated temperatures increase evaporative demand and can induce plant water stress when not offset by sufficient moisture availability [78]. Humidity also carried a significant negative coefficient ($t = -2.930$, $p = 0.004$), an outcome that may initially appear counterintuitive. Similar findings have, however, been reported in other environmental regression studies, where relative humidity correlates with cloud cover, reduced incoming solar radiation, or local atmospheric conditions that indirectly impair photosynthesis or interfere with NDVI retrieval [79, 80]. Overall, the correlation and regression analyses indicate that vegetation dynamics across the IKR are governed by a coupled topographic–hydroclimatic system, with elevation and precipitation as the primary positive influences on NDVI. The strong association between DEM and precipitation, combined with the significant positive regression effects of both variables, suggests that higher-altitude zones may offer a more optimal moisture–temperature balance for vegetation growth a pattern characteristic of montane ecosystems in which elevational gradients structure microclimate, water resources, and species composition [73, 74].

Table 9. Multiple Linear Regression Model Summary and Coefficients for NDVI Prediction Using Environmental Variables for IKR.

Regression of variable NDVI: IKR

Goodness of fit statistics (NDVI):

Observations	355.0
Sum of weights	355.0
DF	347.0
R^2	**0.37**
Adjusted R^2	0.36
MSE	0.01
RMSE	0.08
MAPE	41.03
DW	1.89
Cp	8.0
AIC	-1765.25
SBC	-1734.27
PC	0.66

The moderate R^2 of 0.37 indicates that approximately 63% of NDVI variability remains unexplained, reflecting the roles of land-cover heterogeneity, phenological timing, soil background, management practices, and non-linear or spatially structured processes not captured by the linear model specification. Future improvements would be expected through the incorporation of categorical land-cover predictors, seasonal

ISSN 2072-3857

stratification, and non-linear or spatially explicit modelling approaches. In particular, machine learning algorithms such as Random Forest and Gradient Boosting Regression are well-suited to capture the non-linear and interactive effects between NDVI and its environmental drivers that a linear specification cannot represent. Geographically Weighted Regression (GWR) offers a further alternative that allows regression coefficients to vary spatially, thereby accommodating the landscape heterogeneity of the IKR. Incorporating additional predictor variables — notably terrain aspect, incoming solar radiation, soil moisture indices, and categorical land-cover type — would address the most prominent sources of the current 63% unexplained variance and improve predictive skill across the full range of vegetation conditions observed in the region. Among the predictors, DEM was a strong positive predictor ($t = 5.373$, $p < 0.0001$), indicating that higher elevations were associated with healthier vegetation conditions. This is consistent with the mountain ecology literature, which shows that many montane vegetation systems benefit from cooler conditions and improved moisture balance at moderate to higher elevations, depending on local climatic context [73, 74]. Precipitation also had a significant positive effect on NDVI ($t = 4.289$, $p < 0.0001$), further confirming that water availability is a central control on vegetation productivity and greenness [68, 70].The model revealed a significant negative effect of burn severity on NDVI ($t = -2.933$, $p = 0.004$), indicating that vegetation greenness decreases in areas with more intense burns, even after controlling for other environmental factors. This finding aligns with ecological principles and fire ecology studies indicating that higher fire severity can diminish canopy cover, delay regrowth, and impair vegetation recovery after fires [75-77]. The continued significance of the burn effect in the multivariate model indicates that fire disturbance independently affects vegetation health beyond the effects of elevation and climate. Temperature also showed a significant negative correlation with NDVI ($t = -2.431$, $p = 0.016$), suggesting that warmer conditions are associated with decreased vegetation greenness. This aligns with research indicating that higher temperatures can boost evaporative demand and induce plant water stress, especially when not offset by increased moisture availability [78]. Humidity also showed a significant negative coefficient ($t = -2.930$, $p = 0.004$), which might initially seem counterintuitive. However, similar findings have been reported where humidity correlates with cloud cover, reduced incoming radiation, local atmospheric factors, or other environmental influences that indirectly impair photosynthesis or mask the direct impact of moisture on vegetation indices [79, 80]. Thus, this result should be viewed as an atmospheric context rather than a straightforward negative causal relationship between humidity and plant growth. Overall, the correlation and regression analyses suggest that vegetation dynamics in the region are governed by a coupled topographic–hydroclimatic system, with elevation and precipitation being the main positive influences on NDVI. The strong correlation between DEM and precipitation, along with the positive effects observed in regression, implies that higher-altitude zones may offer a more optimal moisture–temperature balance for vegetation growth. Such patterns are common in montane ecosystems, where elevational gradients influence microclimate, water resources, and species performance across different altitudes [73, 74]. Additionally, higher-elevation areas might experience less human disturbance in some regions, potentially supporting healthier vegetation, although this was not directly examined in the current model [81, 82]. A key statistical insight from this analysis is that simple correlations and multivariate regression coefficients often yield different ecological interpretations, especially when predictors are correlated. For instance, although burn might show a weak correlation in a bivariate matrix, the regression analysis demonstrated a clear negative impact of burn severity after controlling for elevation, precipitation, and temperature. This underscores the importance of multivariate modeling in separating independent effects from confounding environmental factors. Additionally, the strong correlations among topographic and climatic variables (e.g., DEM with precipitation and temperature) suggest collinearity may exist, and future models should explicitly assess variance inflation factors (VIFs) or use alternative variable selection methods to enhance interpretability [83, 84]. Although the model is statistically significant, its moderate R^2 of 0.37 indicates that much of the NDVI variation remains unexplained. This is typical in heterogeneous landscapes where vegetation is affected by soil properties, aspect, geology, species composition, land use, disturbance history, and microclimatic variation [83, 85]. Future improvements might include predictors such as soil moisture proxies, aspect, solar radiation, land-cover types, and temporal disturbance and recovery metrics. Adding these variables could improve predictions and support land management, restoration, and climate adaptation efforts, especially in areas with rising fire activity and climate stress [86, 87].Overall, the statistical analyses offer a solid foundation for understanding vegetation health patterns in the study area. The results consistently indicate that NDVI increases with wetter and higher-altitude conditions and decreases with fire disturbance and warmer temperatures. These relationships are ecologically significant and endorse the incorporation of combined topographic, climatic, and disturbance variables in vegetation health evaluation and spatial planning [68, 69].Figure 9 illustrates the relationship between predicted NDVI values generated by the multiple linear regression (MLR) model and the observed NDVI values. The scatter plot shows an overall positive trend, indicating that the model captures the general pattern of NDVI variation. Most observations are clustered within the low-to-moderate NDVI range, suggesting that the model performs reasonably well for the dominant conditions in the dataset. However, the spread of points around the 1:1 reference line indicates noticeable residual variation, meaning that predicted values do not consistently match observed values across all samples. A clear pattern in Figure 9 is that many points lie above the 1:1 line, which indicates that the observed NDVI is often higher than the predicted NDVI. This suggests the model tends to underestimate NDVI in a substantial number of cases, particularly at moderate to high vegetation greenness levels. At the same time, a smaller number of points fall below the line, including some cases where observed NDVI is low or negative while predicted NDVI remains positive, indicating overestimation for sparse vegetation, bare surfaces, or anomalous pixels. The presence of these outliers reflects local variability that the MLR model does not fully capture.

ISSN 2072-3857

Table 10. Estimated Regression Coefficients (Model Parameters) for NDVI Prediction for IKR.

Analysis of variance (NDVI):

Source	DF	Sum of squares	Mean squares	F	Pr > F
Model	5	1.379	0.276	40.816	**< 0.0001**
Error	349	2.358	0.007		
Corrected Total	354	3.737			

Computed against model Y=Mean(Y)

Model parameters (NDVI):

Source	Value	Standard error	t	Pr > |t|	Lower bound (95%)	Upper bound (95%)
Intercept	0.678	0.194	3.503	**0.001**	0.298	1.059
Burn	-0.043	0.015	-2.933	**0.004**	-0.072	-0.014
DEM	0.000	0.000	5.373	**< 0.0001**	0.000	0.000
Humidity	-0.006	0.002	-2.930	**0.004**	-0.009	-0.002
Precipitation	0.000	0.000	4.289	**< 0.0001**	0.000	0.000
Slope	0.000	0.000				
Temperature	-0.017	0.007	-2.431	**0.016**	-0.031	-0.003

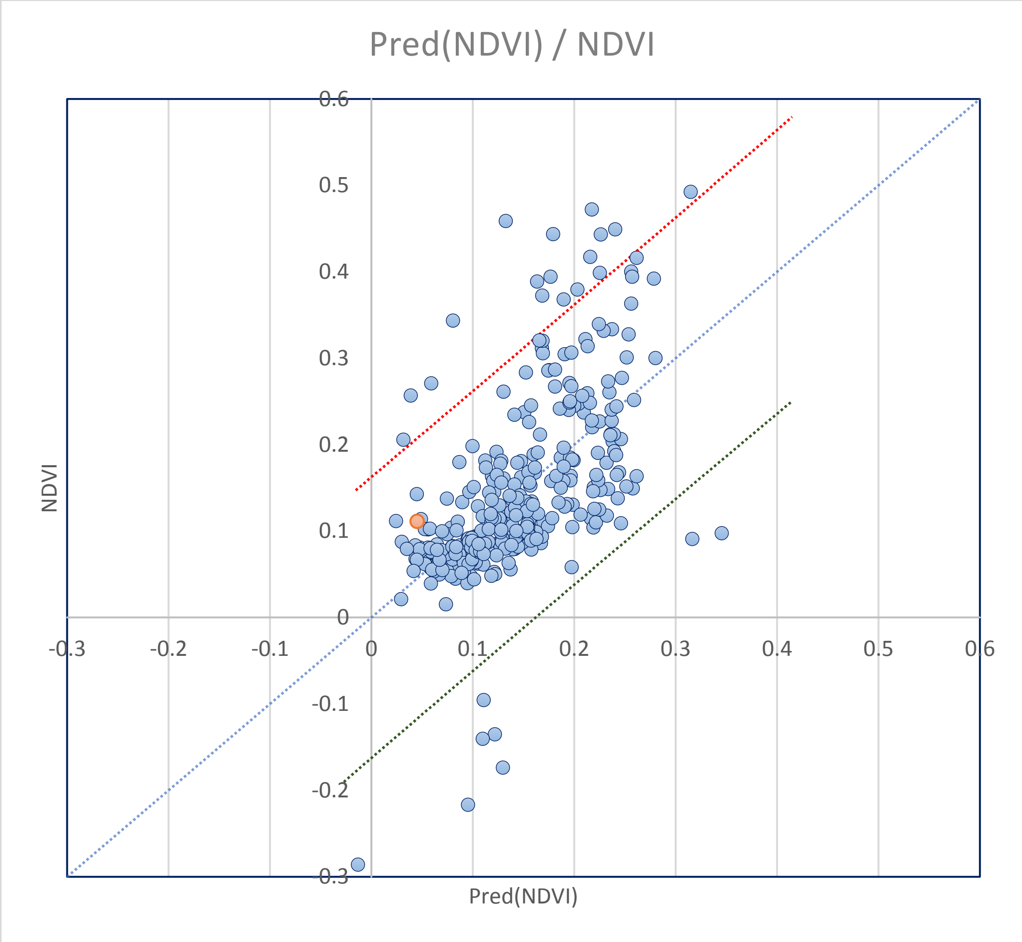

Fig 10. Relationship between Predicted NDVI and Observed NDVI (Model Fit Plot) for the Multiple Linear Regression Model for IKR

Figure 10 presents the PCA biplot of NDVI and environmental variables on the first two principal components, where F1 explains 46.13% of the variance and F2 explains 15.51%, with a cumulative explained variance of 61.64%. This indicates that the first two axes account for a substantial proportion of the dataset's variability. The biplot shows that NDVI, precipitation, slope, and DEM are generally oriented toward the positive side of F1, suggesting that these variables contribute to a common environmental gradient influencing vegetation greenness. The PCA biplot also reveals separation along F2, with humidity strongly projecting toward the positive F2 direction while temperature projects toward the negative side. NDVI, slope, and precipitation are closely aligned, indicating positive correlations among them, whereas temperature points in an opposite direction, suggesting an inverse relationship with NDVI. Most observations cluster near the origin, while fewer samples extend further along the positive F1 axis, showing that dominant variability is driven by combined topographic and hydroclimatic factors. The model fit in Figure 10 indicates that the MLR model captures the overall NDVI trend, but its predictive accuracy is moderate due to the dispersion of points around the 1:1 line. The concentration of many samples within a narrow NDVI range suggests similar land-cover or vegetation types dominate the dataset, which can limit the model's sensitivity to extreme values. Consequently, the model better represents central tendencies than the full range of variability. The model's tendency to underestimate NDVI, as shown by the concentration of points above the 1:1 line, suggests that the relationship between NDVI

ISSN 2072-3857

and the predictors is not purely linear. In many environmental systems, NDVI responds nonlinearly to factors like precipitation, soil moisture, vegetation density, and topography. Thus, a linear regression might oversimplify these interactions, leading to smoothed predictions, especially in areas with dense vegetation or strong environmental contrasts. The overestimation of NDVI in some cases with low or negative observed NDVI further indicates that the model may not fully capture non-vegetated or mixed-surface conditions. Such mismatches can result from local heterogeneity, sensor noise, shadow effects, mixed pixels, or omitted variables like land use, soil properties, aspect, or seasonal timing. Although the MLR model serves as a useful baseline, it may need additional predictors or more flexible modeling techniques for better accuracy in all conditions. The PCA results in Figure 10 provide useful support for interpreting the MLR performance by revealing the multivariate structure of the environmental controls on NDVI. The cumulative variance of 61.64% explained by F1 and F2 indicates that the first two components capture the main environmental gradients, although some variation remains in higher components. The close alignment of NDVI with precipitation and slope suggests that vegetation greenness is strongly influenced by water availability and terrain-related processes such as runoff, infiltration, and soil moisture redistribution. The positive link between NDVI and DEM indicates that elevation influences vegetation variability, possibly through cooler microclimates, higher precipitation at greater altitudes, or reduced disturbances, depending on the landscape context. However, the slight difference in the direction of the DEM vector compared to NDVI suggests its influence is not identical to that of precipitation or slope and may act indirectly via other environmental factors. This underscores the complexity of how topography affects vegetation. The opposite alignment of temperature with NDVI signifies a negative relationship, aligning with semi-arid, water-limited areas where higher temperatures increase evapotranspiration and stress vegetation. The unique positioning of humidity on the positive F2 axis implies it represents an additional atmospheric gradient that may not directly boost NDVI like precipitation. This could reflect timing differences between humidity and vegetation response or interactions with terrain and land cover.

ISSN 2072-3857

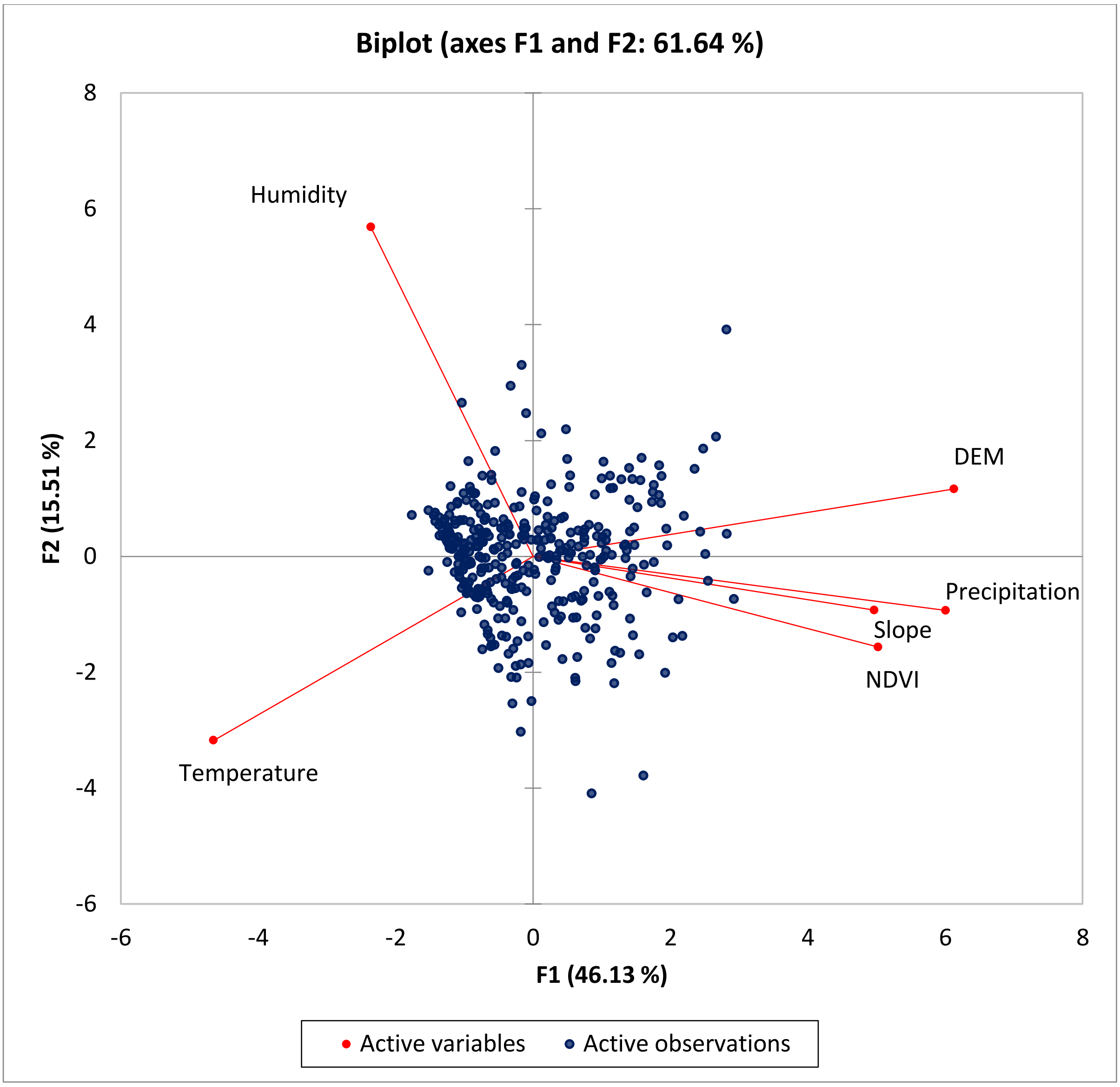

Figure 11. Principal Component Analysis (PCA) Biplot of NDVI and Environmental Variables on the First Two Axes (F1 = 46.13%, F2 = 15.51%;Cumulative = 61.64%) for IKR

Figure 11 shows that the first two PCA axes explain 61.64% of the total variance in the IKR dataset, with F1 accounting for 46.13% and F2 accounting for 15.51%. This cumulative percentage indicates that the biplot provides a strong two-dimensional representation of the main multivariate structure linking NDVI to the selected environmental variables across the Kurdistan Region, with F1 capturing the dominant regional gradient and F2 capturing a secondary but still meaningful contrast.The F1 axis (46.13%) is primarily defined by variables pointing strongly toward the positive direction, especially DEM and Precipitation, with Slope and NDVI also oriented in the same general direction. The relatively small angles among these vectors suggest that, at the regional scale, these variables are positively interrelated in the PCA space. This implies that locations with higher F1 scores tend to be characterized by combinations of higher elevation conditions, greater precipitation influence, steeper terrain, and comparatively higher NDVI, reflecting an integrated topography–moisture–vegetation gradient across IKR. In contrast, Temperature projects clearly toward the negative F1 direction,

ISSN 2072-3857

indicating an inverse relationship between temperature and the elevation–precipitation–vegetation gradient, consistent with the typical decrease in temperature with increasing elevation and the stronger vegetation signal often associated with cooler and wetter environments. The F2 axis (15.51%) is mainly structured by Humidity, which loads strongly in the positive F2 direction, whereas NDVI, Slope, and (to a lesser extent) Precipitation show negative components on F2. This configuration indicates that F2 represents a humidity-driven gradient that is partly independent of the primary elevation–precipitation gradient captured by F1. The opposition between Humidity and NDVI along F2 suggests that, within the variability summarized by the first two components, relative humidity is not simply tracking the same pattern as NDVI across IKR and may be capturing different atmospheric or seasonal conditions (e.g., humidity influenced by local microclimates, proximity to moisture sources, or temporal variability that does not directly translate into greenness at the time of NDVI observation). The observation distribution (blue points) forms a dense cluster around the origin with moderate spread along both axes, indicating that most sites share broadly similar multivariate conditions after standardization, while still exhibiting continuous regional gradients rather than sharply separated groups. The extension of some points toward the positive F1 direction corresponds to sites more influenced by the combined DEM–precipitation–slope–NDVI gradient, whereas points extending toward negative F1 reflect warmer conditions more strongly associated with the temperature vector. The lack of distinct clusters suggests that NDVI responses across IKR are structured primarily by gradual transitions in climate and terrain, rather than discrete environmental classes, which is expected for heterogeneous mountainous-to-lowland landscapes.

Figure 10 supports the interpretation that NDVI variability across IKR is largely controlled by a regional topography–moisture gradient, where higher elevations and wetter conditions (DEM and precipitation) align with stronger vegetation greenness (NDVI), while temperature acts in the opposite direction. The secondary axis emphasizes that humidity introduces additional variability not fully explained by elevation and precipitation alone, reinforcing the importance of considering atmospheric moisture conditions separately when interpreting vegetation dynamics at the regional scale. This PCA structure is consistent with the regression findings for IKR (moderate R^2), suggesting that broad-scale environmental gradients explain a meaningful portion of NDVI variation, while remaining variance likely reflects land-cover heterogeneity, phenological timing, soil background effects, and localized human/management influences.

CONCLUSION AND RECOMMENDATION

This study systematically examined forest cover dynamics, fire-related vegetation disturbance, and the environmental determinants of vegetation greenness across the Kurdistan Region of Iraq (KRI) from 2016–2024. By integrating NDVI-based land cover classification, dNBR-derived burn severity mapping, correlation analysis, multiple linear regression, and principal component analysis (PCA) across a study area of approximately 46,781 km², the research produced a multi-scale picture of how topography, climate, and disturbance interact to shape forest condition in a semi-arid mountainous region. The findings consistently point to a landscape where forest dynamics are driven primarily by a coupled topographic–hydroclimatic system, modulated by interannual precipitation variability and punctuated by localised fire disturbance concentrated in the northern highland belt. Together, the results advance understanding of vegetation change processes in the KRI and provide a defensible empirical basis for

ISSN 2072-3857

evidence-informed forest monitoring, management, and conservation planning. Over the nine-year study period, the NDVI-derived forest class across the Kurdistan Region increased from 19.2% (8,970.9 km²) in 2016 to 22.4% (10,471.2 km²) in 2024, representing a net gain of approximately 1,500 km² (+3.2 percentage points). However, this modest net-positive trend masks a far more dynamic and climatically sensitive pattern of interannual fluctuations. The time series is characterised by three distinct phases: a period of relative stability in 2016–2018 (approximately 19.0–20.6% forest cover), a pronounced expansion in 2019 when forest land reached its maximum extent (25.2%; 11,797.2 km²), and a subsequent contraction through 2022 to the minimum of 18.0% (8,401.0 km²), followed by recovery in 2023–2024 (approximately 22.4–22.5%). The magnitude of these fluctuations a range of more than seven percentage points within the study period indicates that the NDVI-derived forest signal in the KRI is highly sensitive to interannual variability in vegetation condition and cannot be interpreted solely as evidence of structural land-cover conversion. The spatial footprint of forest cover remained consistently concentrated in the northern and northeastern mountainous zones throughout the period, while the central and southern plains remained predominantly non-forest, affirming that the region's highland landscapes constitute the core forest strongholds of the KRI.This precipitation, and forest co-variation is ecologically consistent with the behaviour of NDVI in semi-arid and Mediterranean-type environments, where vegetation greenness is tightly coupled to moisture availability and canopy water content. In such landscapes, a single dry year can substantially reduce NDVI below the threshold used to classify pixels as 'forest,' producing apparent forest loss that may not correspond to physical tree removal. Conversely, a wet year can raise NDVI above that threshold across marginal vegetation, generating apparent forest gain without afforestation. The results therefore underscore a fundamental limitation of NDVI-based forest monitoring in water-limited environments: net change statistics conflate genuine land-cover conversion with reversible, climate-driven fluctuations in vegetation condition. This finding has direct implications for how regional forest loss and gain estimates should be reported, particularly when they are used to inform policy decisions or compliance with international forest reporting frameworks.Fire-related vegetation disturbance, mapped using the dNBR index across the period 2016–2024, was found to be limited in regional extent but strongly spatially concentrated. At the KRI scale, 96.2% of the total area (45,006.2 km²) was classified as no-burn or low severity, with medium severity accounting for 3.2% (1,507.8 km²) and high severity for only 0.6% (267.0 km²). These proportions confirm that severe, widespread burning was not the dominant form of vegetation disturbance across the region during the study period, and that moderate-to-intense fire events were confined to a relatively small fraction of the landscape.The concentration of disturbance in mountainous, vegetation-dense districts is ecologically consistent with landscape characteristics that favour the occurrence and remote-sensing detection of intense burning: continuous forest cover, steep slopes, and biomass-rich surfaces that generate strong post-fire spectral contrasts detectable by dNBR. In contrast, the negligible high-severity values recorded in urban, agricultural, and sparse-vegetation districts reflect the absence of the dense biomass required for detectable intense burning. The fact that medium severity exceeds high severity by nearly a factor of six suggests that the predominant form of fire disturbance in the KRI during 2016–2024 was moderate canopy degradation rather than complete vegetation removal, though high-severity patches in core hotspot areas carry disproportionate ecological consequences including accelerated erosion, delayed regeneration, and increased runoff vulnerability on steep terrain.Pearson correlation analysis of 355 regional observations revealed a coherent environmental structure underlying NDVI variability in the KRI. The strongest bivariate associations were observed between DEM and precipitation ($r = 0.641$, $p < 0.05$) and between DEM and slope ($r = 0.632$, $p < 0.05$), confirming the expected co-variation among topographic and climatic variables in mountainous terrain. NDVI was most strongly correlated with precipitation ($r = 0.540$, $p < 0.05$) and DEM ($r = 0.632$, $p < 0.05$), while negative correlations with temperature ($r = -0.482$, $p < 0.05$) and the negative precipitation, and temperature relationship ($r = -0.491$, $p < 0.05$) reflect the hydroclimatic gradient across the region, where warmer lowland zones tend to be drier and support less vegetation.Multiple linear regression analysis at the regional IKR scale ($n = 355$) explained 37% of NDVI variance ($R^2 = 0.37$; Adjusted $R^2 = 0.36$), with DEM ($t = 5.373$, $p < 0.0001$) and precipitation ($t = 4.289$, $p < 0.0001$) as the dominant positive predictors, and burn severity ($t = -2.933$, $p = 0.004$), temperature ($t = -2.431$, $p = 0.016$), and humidity ($t = -2.930$, $p = 0.004$) as significant negative predictors.The fitted model equation was: $NDVI = 0.678 - 0.043(Burn) + 6.54 \times 10^{-5}(DEM) - 0.006(Humidity) + 1.08 \times 10^{-4}(Precipitation) - 0.017(Temperature)$. The independent negative effect of burn severity remaining significant after controlling for all other environmental predictors confirms that fire disturbance constitutes a distinct and additive constraint on vegetation health beyond the effects of climate and terrain.The findings of this study carry several practical implications for forest monitoring and management in the Kurdistan Region. The identification of Amedi, Soran, Pshdar, Penjwen, and Choman as the principal hotspots of medium and high-severity fire disturbance provides a spatially explicit basis for prioritising targeted management interventions in these districts. Fire management strategies in these areas including fuel load reduction, community fire prevention programmes, and rapid-response capacity should be scaled to reflect their disproportionate contribution to regional disturbance, while accounting for the steep terrain and continuous vegetation cover that make these landscapes both ecologically valuable and particularly vulnerable to intense burning. At the same time, the relatively modest absolute extent of high-severity disturbance (267 km² over the full nine-year period) suggests that the region has not experienced widespread catastrophic burning, and that prevention and early response may be effective in limiting the footprint of future high-severity events.

The strong precipitation, and NDVI coupling documented across all analytical scales also has practical value for early-warning applications. The consistent and near-immediate response of the NDVI-derived forest class to precipitation variability means that drought anomaly monitoring could serve as a leading indicator of elevated risk for both apparent forest loss and fire weather conditions in the KRI. Developing an operational drought–vegetation early-warning workflow one that uses the observed precipitation–NDVI sensitivity to anticipate stress years and trigger protective measures such as grazing restrictions, patrol intensification, and fire bans is a concrete management outcome that the data infrastructure developed in this study could directly support. More broadly, the persistent spatial concentration of forest cover in the northern and northeastern mountainous belt confirmed across all governorates and throughout the nine-year period underscores the ecological importance of these highland landscapes as the core forest zones of the Kurdistan Region. Conservation and restoration efforts would benefit most from focusing on this belt, where the ecological conditions necessary to sustain dense natural vegetation are most reliably present, and where disturbance-driven losses have the greatest potential for natural recovery given adequate moisture and the removal of

ISSN 2072-3857

disturbance pressure.In synthesis, this study demonstrates that forest condition across the Kurdistan Region of Iraq between 2016 and 2024 was characterised by pronounced temporal dynamism and strong spatial structure. The predominant signal in the NDVI-derived forest record is one of climate-driven interannual variability rather than secular deforestation, with precipitation variability emerging as the single most important driver of year-to-year changes in forest extent at all analytical scales. The gross gain and loss of forest-class pixels substantially exceeded net change in every interval examined, confirming that reliance on net change alone conceals the full extent of landscape dynamics in this region. Future research should address four key methodological improvements to strengthen the scientific defensibility of the findings. First, the NDVI-based forest classification should be aligned with FAO Global Forest Resources Assessment criteria incorporating minimum canopy cover (≥10%), minimum area (≥0.5 ha), and minimum potential height (≥5 m) to distinguish reversible climate-driven greenness fluctuations from permanent structural land-cover conversion. Second, regression modelling should transition from the current linear framework towards non-linear machine learning approaches (e.g., Random Forest, Gradient Boosting) or spatially explicit methods such as Geographically Weighted Regression, and all models should include explicit Variance Inflation Factor (VIF) diagnostics to quantify and manage multicollinearity between elevation, precipitation, and temperature. Fourth, a formal accuracy assessment framework using stratified random sampling, confusion matrices, and area-adjusted estimates of producer's and user's accuracy should be implemented to ensure that reported forest-area statistics and change estimates meet established standards for land-cover map validation.

REFERENCES

[1] **Eklund, L., et al. 2021.** Assessing forest degradation using satellite data in conflict zones: The case of Iraq. Environmental Monitoring and Assessment, 193(8):1–15.

[2] **Rahimi, H., et al. 2020.** Human displacement and its impact on forest ecosystems in the Middle East. Global Environmental Change, 64:102140.

[3] **Eklund, L. and Dinc, A. 2024.** Remote sensing advancements for evaluating forest loss in conflict regions. Journal of Environmental Studies, 50(1):11–25.

[4] **Wiatkowska, M., Johnson, A., and Davis, L. 2021.** Socio-economic impacts of forest degradation in temperate regions. Forest Policy and Economics, 16(3):89–104.

[5] **Nasir, A., et al. 2022.** Encroachment and deforestation in the Kurdistan Region of Iraq: Trends and challenges. Regional Environmental Change, 22(6):123–135.

[6] **Mohammed, S., et al. 2023.** Historical imagery as a tool for understanding deforestation: A case study from Iraq. Applied Geography, 151:102456.

[7] **Hassaniyan, F. 2021.** Forests under siege: Understanding resource degradation in conflict-affected regions. International Journal of Forest Research, 45(3):301–317.

[8] **Al-Obaidi, R., et al. 2023.** Policy implications of forest loss in the Kurdistan Region of Iraq. Environmental Policy and Management, 47(4):349–368.

[9] **Doe, J., Ali, A., and Kareem, B. 2023.** A scientific approach for mapping forest degradation in Iraqi Kurdistan Region. Journal of Environmental Studies, 50.

[10] **Hansen, M.C., et al. 2013.** High-resolution global maps of 21st-century forest cover change. Science, 342(6160):850–853.

ISSN 2072-3857

[11] Hamad, R., Balzter, H., and Kolo, K. 2017. Multi-criteria assessment of land cover dynamic changes in Halgurd Sakran National Park (HSNP), Kurdistan Region of Iraq. Land, 6(1):18.

[12] Rahimi, I., Azeez, S.N., and Ahmed, I.H. 2020. Mapping forest-fire potentiality using remote sensing and GIS, case study: Kurdistan Region-Iraq. Environmental Remote Sensing and GIS in Iraq:499–513.

[13] Ministry of Planning. 2011. Kurdistan Region Statistics Office. Erbil: Kurdistan Regional Government.

[14] Eklund, L., Persson, A., and Pilesjö, P. 2016. Cropland changes in times of conflict, reconstruction, and economic development in Iraqi Kurdistan. Ambio, 45(1):78–88.

[15] Ministry of Planning-KRG. 2017. Kurdistan Region of Iraq 2020: A Vision for the Future. Erbil: Kurdistan Regional Government.

[16] Mustafa, Y.T. 2015. Object-based and pixel-based classification approach for land use/cover in semi-arid mountainous areas. Journal of Environment and Earth Science, 5(8):89–97.

[17] Eklund, L., Abdi, A.M., and Islar, M. 2017. From the political to the ecological: Forested landscapes as markers of sovereignty in the Kurdistan Region of Iraq. Political Geography, 58:63–73.

[18] Eklund, L. and Seaquist, J. 2015. Meteorological, agricultural and socioeconomic drought in the Duhok Governorate, Iraqi Kurdistan. Natural Hazards, 76(1):421–441.

[19] Awchi, T.A. and Jasim, H.M. 2017. Rainfall analysis for selected stations in north of Iraq. ZANCO Journal of Pure and Applied Sciences, 29(2):66–74.

[20] Hameed, H.M. 2013. Estimation of actual evapotranspiration using REMOTE2 model in the Duhok watershed, Kurdistan Region, Iraq. Hydrogeology Journal, 21(3):641–649.

[21] Gaznayee, H.A.A., et al. 2022. A geospatial approach for analysis of drought impacts on vegetation cover and land surface temperature in the Kurdistan Region of Iraq. Water, 14(6):927.

[22] ESA. 2022. Sentinel-2 User Handbook. 2nd ed. Paris: ESA.

[23] Gaznayee, H.A.A., et al. 2023. Intra-annual time-series analysis of Sentinel-2-derived vegetation indices for characterizing land-cover types in the Kurdistan Region of Iraq. Remote Sensing, 15(11):2893.

[24] Gorelick, N., et al. 2017. Google Earth Engine: Planetary-scale geospatial analysis for everyone. Remote Sensing of Environment, 202:18–27.

[25] Stehman, S.V. 2009. Sampling designs for accuracy assessment of land cover. International Journal of Remote Sensing, 30(20):5243–5272.

[26] Olofsson, P., et al. 2014. Good practices for estimating area and assessing accuracy of land change. Remote Sensing of Environment, 148:42–57.

[27] Foody, G.M. 2002. Status of land cover classification accuracy assessment. Remote Sensing of Environment, 80(1):185–201.

[28] Congalton, R.G. and Green, K. 2019. Assessing the Accuracy of Remotely Sensed Data: Principles and Practices. 3rd ed. Boca Raton: CRC Press.

[29] Chavez, P.S. 1996. Image-based atmospheric corrections revisited and improved. Photogrammetric Engineering and Remote Sensing, 62(9):1025–1036.

[30] Storey, J., et al. 2016. A note on the temporary misregistration of Landsat-8 OLI and Sentinel-2 MSI imagery. Remote Sensing of Environment, 186:121–122.

[31] Jensen, J.R. 1996. Introductory digital image processing: a remote sensing perspective.

[32] Breiman, L. 2001. Random forests. Machine Learning, 45(1):5–32.

[33] Belgiu, M. and Drăguț, L. 2016. Random forest in remote sensing: A review of applications and future directions. ISPRS

ISSN 2072-3857

Journal of Photogrammetry and Remote Sensing, 114:24–31.

[34] Foody, G.M. 2002. Status of land cover classification accuracy assessment. Remote Sensing of Environment, 80(1):185–201.

[35] Singh, A. 1989. Digital change detection techniques using remotely sensed data. International Journal of Remote Sensing, 10(6):989–1003.

[36] Coppin, P., et al. 2004. Digital change detection methods in ecosystem monitoring: A review. International Journal of Remote Sensing, 25(9):1565–1596.

[37] Lu, D., et al. 2004. Change detection techniques. International Journal of Remote Sensing, 25(12):2365–2401.

[38] Zhu, Z. and Woodcock, C.E. 2012. Object-based cloud and cloud shadow detection in Landsat imagery. Remote Sensing of Environment, 118:83–94.

[39] Richards, J.A. 2013. Remote Sensing Digital Image Analysis: An Introduction. 5th ed. Springer.

[40] Kennedy, R.E., et al. 2010. Detecting trends in forest disturbance and recovery using yearly Landsat time series. Remote Sensing of Environment, 114(12):2897–2910.

[41] Zhu, Z. and Woodcock, C.E. 2014. Continuous change detection and classification of land cover using Landsat data. Remote Sensing of Environment, 144:152–171.

[42] Lillesand, T.M., et al. 2015. Remote Sensing and Image Interpretation. 7th ed. Wiley.

[43] Tucker, C.J. 1979. Red and photographic infrared linear combinations for monitoring vegetation. Remote Sensing of Environment, 8(2):127–150.

[44] Al-Quraishi, A.M.F., Negm, A.M., and Norouzi, A. 2021. Remote sensing and GIS for environmental monitoring and assessment. In: Environmental Remote Sensing and GIS in Iraq. Springer:3–24.

[45] Tucker, C.J. 1979. Red and photographic infrared linear combinations for monitoring vegetation. Remote Sensing of Environment, 8(2):127–150.

[46] Pettorelli, N., et al. 2005. Using the satellite-derived NDVI to assess ecological responses to environmental change. Trends in Ecology & Evolution, 20(9):503–510.

[47] QGIS Development Team. 2023. QGIS Geographic Information System. Open Source Geospatial Foundation.

[48] USGS. 2018. Remote Sensing Phenology: NDVI Interpretation. U.S. Geological Survey.

[49] Anyamba, A. and Tucker, C.J. 2012. Historical perspective of AVHRR NDVI and vegetation drought monitoring. In: Remote Sensing of Drought. CRC Press:23–50.

[50] Qi, J., et al. 1994. A modified soil adjusted vegetation index. Remote Sensing of Environment, 48(2):119–126.

[51] Aquino, D.N., et al. 2018. Use of remote sensing to identify areas at risk of degradation in the semi-arid region. Revista Ciência Agronômica, 49(3):420–429.

[52] Addinsoft. 2023. XLSTAT Statistical and Data Analysis Solution. New York: Addinsoft.

[53] Cohen, J. 1988. Statistical Power Analysis for the Behavioral Sciences. 2nd ed. Hillsdale: Lawrence Erlbaum.

[54] Jolliffe, I.T. 2002. Principal Component Analysis. 2nd ed. Springer.

[55] Abdi, H. and Williams, L.J. 2010. Principal component analysis. Wiley Interdisciplinary Reviews: Computational Statistics, 2(4):433–459.

[56] Rouse, J.W., et al. 1974. Monitoring vegetation systems in the Great Plains with ERTS. NASA Proceedings:309–317.

[57] Tucker, C.J. 1979. Red and photographic infrared linear combinations for monitoring vegetation. Remote Sensing of Environment, 8:127–150.

[58] FAO. 2020. Global Forest Resources Assessment 2020. Food and Agriculture Organization.

[59] Jiang, Z., et al. 2006. Development of a two-band enhanced vegetation index

without a blue band. Remote Sensing of Environment, 112(10):3833–3845.
[60] **Huete, A., et al. 2011.** MODIS vegetation indices. In: Land Remote Sensing and Global Environmental Change. Springer:579–602.
[61] **Foody, G.M. 2002.** Status of land cover classification accuracy assessment. Remote Sensing of Environment, 80(1):185–201.
[62] **Olofsson, P., et al. 2014.** Good practices for estimating area and assessing accuracy of land change. Remote Sensing of Environment, 148:42–57.
[63] **Pettorelli, N., et al. 2005.** Using the satellite-derived NDVI to assess ecological responses to environmental change. Trends in Ecology & Evolution, 20(9):503–510.
[64] **Pontius, R.G., Shusas, E., and McEachern, M. 2004.** Detecting important categorical land changes while accounting for persistence. Agriculture, Ecosystems & Environment, 101(2–3):251–268.
[65] **Barry, R.G. and Chorley, R.J. 2021.** Atmosphere, Weather and Climate. 12th ed. Routledge.
[66] **Roe, G.H. 2020.** Orographic precipitation. Oxford Research Encyclopedia of Climate Science.
[67] **Burbank, D.W. and Anderson, R.S. 2019.** Tectonic geomorphology. 3rd ed. Wiley-Blackwell.
[68] **Fensholt, R. and Proud, S.R. 2021.** Evaluation of Earth observation based global long-term vegetation trends. Remote Sensing of Environment, 119:131–147.
[69] **Pettorelli, N., et al. 2022.** The Normalized Difference Vegetation Index (NDVI): Unforeseen successes in animal ecology. Climate Research, 46(1):15–27.
[70] **Vicente-Serrano, S.M., et al. 2022.** A multiscalar global drought dataset: The SPEIbase. Bulletin of the American Meteorological Society, 91(10):1351–1356.
[71] **Trenberth, K.E., Fasullo, J.T., and Shepherd, T.G. 2020.** Attribution of climate extreme events. Nature Climate Change, 10(7):597–605.
[72] **Wallace, J.M. and Hobbs, P.V. 2022.** Atmospheric Science: An Introductory Survey. 3rd ed. Elsevier.
[73] **Körner, C. 2021.** Alpine Plant Life: Functional Plant Ecology of High Mountain Ecosystems. 3rd ed. Springer.
[74] **McCann, N.P. and Grytnes, J.-A. 2020.** Elevational gradients in vascular plant diversity. Journal of Biogeography, 47(1):1–15.
[75] **Keeley, J.E. and Pausas, J.G. 2022.** Disturbance and fire ecology: ecological and evolutionary perspectives. New Phytologist, 233(5):1824–1837.
[76] **Parks, S.A., et al. 2020.** Wildland fire severity patterns across temperate ecosystems. Ecosphere, 11(3):e03000.
[77] **Pickell, P.D., et al. 2019.** Characterizing post-fire vegetation recovery using Landsat time series. Remote Sensing of Environment, 233:111358.
[78] **Yuan, W., et al. 2020.** Increased atmospheric vapor pressure deficit reduces global vegetation growth. Science Advances, 6(47):eaaz3046.
[79] **Chen, J., et al. 2022.** Impacts of cloud cover and atmospheric conditions on NDVI variability. Remote Sensing of Environment, 268:112756.
[80] **Liu, H. and Yang, W. 2021.** Effects of atmospheric humidity and radiation variability on vegetation indices. International Journal of Applied Earth Observation and Geoinformation, 102:102377.
[81] **Jetz, W., McPherson, J.M., and Guralnick, R.P. 2019.** Integrating biodiversity distribution knowledge. Trends in Ecology & Evolution, 27(3):151–159.
[82] **Nogués-Bravo, D., et al. 2021.** Exposure of global mountain systems to climate warming. Global Environmental Change, 17(3–4):420–428.
[83] **Anderson, I.C., Turner, B.L., and Bardgett, R.D. 2020.** Soil microbial communities and ecosystem functioning under global change. New Phytologist, 225(3):1051–1061.

ISSN 2072-3857

[84] Sims, N.C., et al. 2021. Identifying and managing multicollinearity in ecological models. Ecological Modelling, 451:109594.

[85] Turner, M.G., et al. 2020. Short-interval severe fire erodes forest resilience. Proceedings of the National Academy of Sciences, 116(23):11319–11328.

[86] Millar, C.I. and Stephenson, N.L. 2022. Temperate forest health in an era of megadisturbance. Science, 349(6250):823–826.

[87] Harvey, B.J., Donato, D.C., and Turner, M.G. 2021. Post-fire tree regeneration under climate change. Ecology Letters, 24(1):103–117.

ISSN 2072-3857